JCI The Journal of Clinical Investigation

Group III secreted phospholipase A_2 regulates epididymal sperm maturation and fertility in mice

Hiroyasu Sato, … , Ichiro Kudo, Makoto Murakami

J Clin Invest. 2010;120(5):1400-1414. https://doi.org/10.1172/JCI40493.

Research Article

Although lipid metabolism is thought to be important for the proper maturation and function of spermatozoa, the molecular mechanisms that underlie this dynamic process in the gonads remains incompletely understood. Here, we show that group III phospholipase A_2 (sPLA$_2$-III), a member of the secreted phospholipase A_2 (sPLA$_2$) family, is expressed in the mouse proximal epididymal epithelium and that targeted disruption of the gene encoding this protein (*Pla2g3*) leads to defects in sperm maturation and fertility. Although testicular spermatogenesis in *Pla2g3*$^{-/-}$ mice was grossly normal, spermatozoa isolated from the cauda epididymidis displayed hypomotility, and their ability to fertilize intact eggs was markedly impaired. Transmission EM further revealed that epididymal spermatozoa in *Pla2g3*$^{-/-}$ mice had both flagella with abnormal axonemes and aberrant acrosomal structures. During epididymal transit, phosphatidylcholine in the membrane of *Pla2g3*$^{+/+}$ sperm underwent a dramatic shift in its acyl groups from oleic, linoleic, and arachidonic acids to docosapentaenoic and docosahexaenoic acids, whereas this membrane lipid remodeling event was compromised in sperm from *Pla2g3*$^{-/-}$ mice. Moreover, the gonads of *Pla2g3*$^{-/-}$ mice contained less 12/15-lipoxygenase metabolites than did those of *Pla2g3*$^{+/+}$ mice. Together, our results reveal a role for the atypical sPLA$_2$ family member sPLA$_2$-III in epididymal lipid homeostasis and indicate that its perturbation may lead to sperm dysfunction.

Group III secreted phospholipase A_2 regulates epididymal sperm maturation and fertility in mice

Hiroyasu Sato,[1,2] Yoshitaka Taketomi,[1,3] Yuki Isogai,[1,4] Yoshimi Miki,[1,2] Kei Yamamoto,[1] Seiko Masuda,[1,2] Tomohiko Hosono,[3] Satoru Arata,[3] Yukio Ishikawa,[5] Toshiharu Ishii,[5] Tetsuyuki Kobayashi,[4,6] Hiroki Nakanishi,[6,7] Kazutaka Ikeda,[6,7] Ryo Taguchi,[6,7] Shuntaro Hara,[2] Ichiro Kudo,[2] and Makoto Murakami[1,8]

[1]Biomembrane Signaling Project, Tokyo Metropolitan Institute of Medical Science, Tokyo, Japan. [2]Department of Health Chemistry, School of Pharmaceutical Sciences, and [3]Center for Biotechnology, Showa University, Tokyo, Japan. [4]Department of Biology, Faculty of Science, Ochanomizu University, Tokyo, Japan. [5]Department of Pathology, Toho University School of Medicine, Tokyo, Japan. [6]Core Research for Evolutional Science and Technology (CREST), Japan Science and Technology Agency, Kawaguchi, Japan. [7]Department of Metabolome, Graduate School of Medicine, The University of Tokyo, Tokyo, Japan. [8]Precursory Research for Embryonic Science and Technology (PRESTO), Japan Science and Technology Agency, Kawaguchi, Japan.

Although lipid metabolism is thought to be important for the proper maturation and function of spermatozoa, the molecular mechanisms that underlie this dynamic process in the gonads remains incompletely understood. Here, we show that group III phospholipase A_2 (sPLA$_2$-III), a member of the secreted phospholipase A_2 (sPLA$_2$) family, is expressed in the mouse proximal epididymal epithelium and that targeted disruption of the gene encoding this protein (*Pla2g3*) leads to defects in sperm maturation and fertility. Although testicular spermatogenesis in *Pla2g3*$^{-/-}$ mice was grossly normal, spermatozoa isolated from the cauda epididymidis displayed hypomotility, and their ability to fertilize intact eggs was markedly impaired. Transmission EM further revealed that epididymal spermatozoa in *Pla2g3*$^{-/-}$ mice had both flagella with abnormal axonemes and aberrant acrosomal structures. During epididymal transit, phosphatidylcholine in the membrane of *Pla2g3*$^{+/+}$ sperm underwent a dramatic shift in its acyl groups from oleic, linoleic, and arachidonic acids to docosapentaenoic and docosahexaenoic acids, whereas this membrane lipid remodeling event was compromised in sperm from *Pla2g3*$^{-/-}$ mice. Moreover, the gonads of *Pla2g3*$^{-/-}$ mice contained less 12/15-lipoxygenase metabolites than did those of *Pla2g3*$^{+/+}$ mice. Together, our results reveal a role for the atypical sPLA$_2$ family member sPLA$_2$-III in epididymal lipid homeostasis and indicate that its perturbation may lead to sperm dysfunction.

Introduction

The male reproductive system consists of a series of organs that act together to produce and deliver functional spermatozoa into the female reproductive tract. After the complex differentiation process of male germ cells, spermatozoa exit the seminiferous tubules of the testis through the efferent ducts toward the epididymis. During their transit from the caput to the cauda epididymidis, spermatozoa undergo significant morphological and biochemical modifications, which lead to acquisition of their forward motility and ability to recognize and fertilize oocytes (1). Since 1 out of 6 couples of reproductive age present with infertility, understanding of the molecular mechanisms underlying the proper development of gametes in the gonadal niche is of considerable biomedical and clinical importance.

A number of knockout mouse models have been reported to display reproduction disorders, among which, those harboring abnormalities of lipid metabolism are often accompanied by fertility defects. For instance, disruption of several genes regulated for the biosynthesis or receptors for arachidonic acid–derived eicosanoids perturbs the reproduction process in females rather than in males (2–5). In contrast, knockout of genes affecting lipid signaling (6, 7) and transport (8–11) often profoundly affects the maturation and function of spermatozoa. In addition, accumulating evidence suggests that composition changes of sperm lipids can affect sperm quality and functions (12). Rodents fed an essential fatty acid–deficient diet or those unable to synthesize polyunsaturated fatty acids (PUFAs) show degeneration of germ cells (13). Inactivation of genes involved in the synthesis or transport of PUFAs hampers fertilization, even in invertebrates such as *Drosophila* and *Caenorhabditis elegans* (14, 15).

Amounts of cholesterol and phospholipids are lower in mature and motile sperm than in immature and immotile sperm of both human and mouse species (16, 17). A quality unique to mammalian sperm cells is the abundance of phospholipid species with C22-PUFAs, particularly docosahexaenoic acid (DHA; an ω-3 fatty acid), whose proportion in membrane phospholipids appears to correlate with sperm maturity, motility, and fertility (17–20). In humans, the percentage of DHA relative to total fatty acids is correlated with the normal morphology of sperm cells, whereas an inverse relationship between the percentage of atypical sperm cells and that of DHA is seen (19). Sperm cells from subfertile men with low sperm motility or counts contain a percentage of DHA lower than that from normal men (21). Sperm maturation involves the remodeling of membrane phospholipids toward the acquisition of motility and fertility during sperm migration through the epididymis. Indeed, the increase in C22-PUFAs, such as DHA and docosapentaenoic acid (DPA), and the reciprocal decrease in ω-6 arachidonic acid favor an increase in the unsaturation degree of fatty acids in mouse sperm membrane during epididymal transit (17), which could consequently contribute to increasing the mouse sperm membranous fluidity, as it was

Conflict of interest: The authors have declared that no conflict of interest exists.
Citation for this article: *J Clin Invest.* 2010;120(5):1400–1414. doi:10.1172/JCI40493.

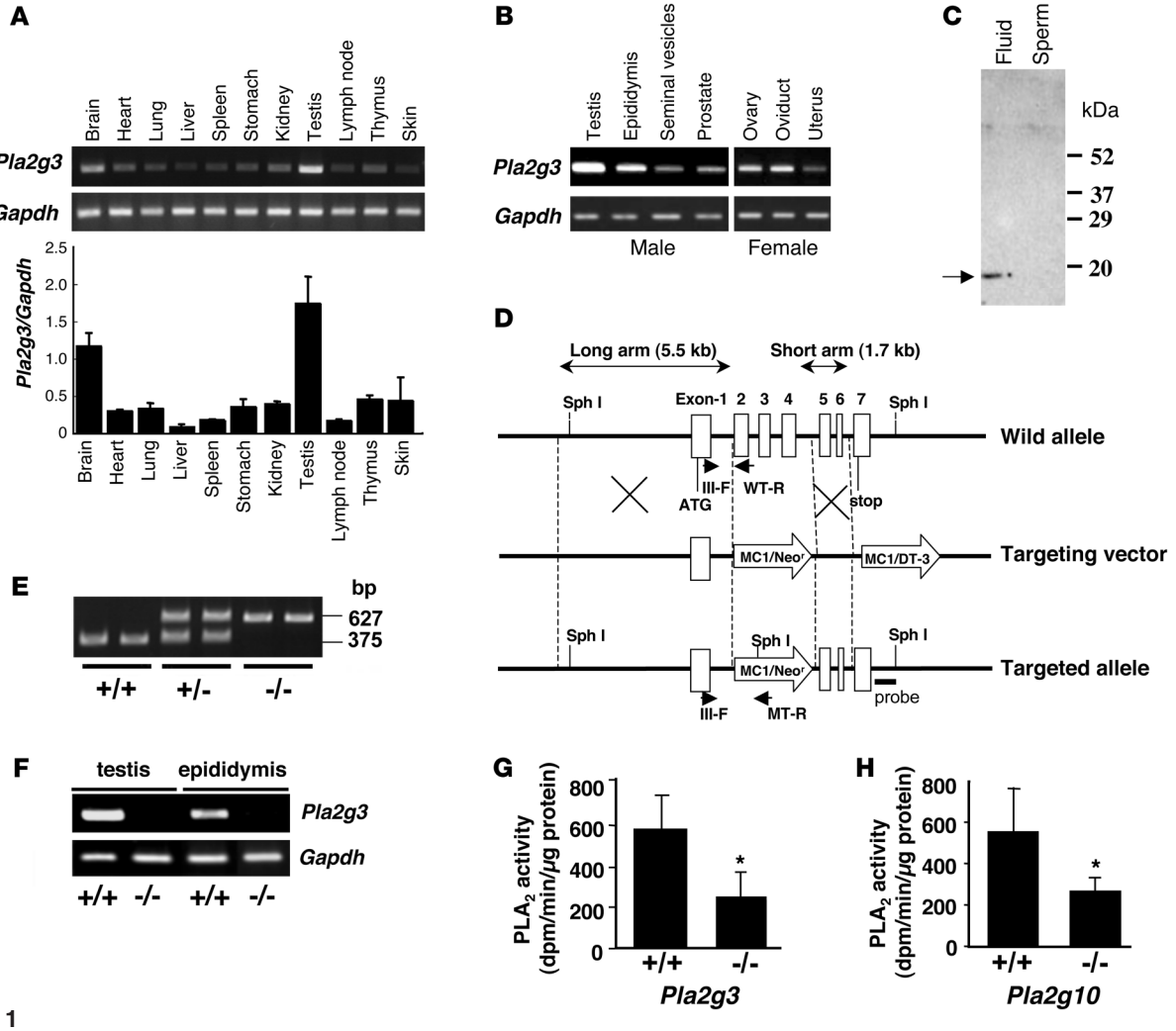

Figure 1

Targeted disruption of the *Pla2g3* gene. (**A**) Expression of transcripts for *Pla2g3* in various tissues of male C57BL/6 mice was assessed using RT-PCR. After electrophoresis of the PCR products in agarose gels with ethidium bromide (top panel), the intensities of the band for *Pla2g3*, relative to those for *Gapdh*, were quantified using a densitometer (CS analyzer 2.0; mean ± SD; $n = 3$) (bottom panel). (**B**) RT-PCR of *Pla2g3* mRNA expression in male and female reproductive organs from C57BL/6 mice. (**C**) Immunoblotting of $sPLA_2$-III protein in sperm and fluid from the cauda epididymidis of C57BL/6 mice. Arrow indicates a fully processed $sPLA_2$-III. (**D**) Schematic representation of the *Pla2g3* gene, targeting vector, and mutated *Pla2g3* allele. Details of the construction of the targeting vector are given in Methods. Arrows indicate positions of primers for PCR genotyping. Boxes indicate exons of the *Pla2g3* gene. Large arrows indicate the 5.5-kb long-arm and 1.7-kb short-arm genomic fragments of the *Pla2g3* gene. Small arrows indicate the positions of primers used for PCR genotyping (III-F, WT-R, and MT-R indicate Pla2g3 WT forward primer, WT reverse primer, and mutant reverse primer, respectively). "X" indicates the regions where homologous recombination occurs. A bold bar shows a region used as a probe for Southern blotting. (**E**) Genotyping using PCR of samples from mouse tails. The WT and mutant alleles gave 375-bp and 627-bp amplified fragments, respectively. (**F**) Confirmation by RT-PCR of the absence of *Pla2g3* mRNA in the testis and epididymis of nullizygous mice. (**G**) PLA_2 enzymatic activity in cauda epididymal fluid of *Pla2g3*$^{-/-}$ mice and their littermates. (**H**) PLA_2 enzymatic activity in cauda epididymal fluid of *Pla2g10*$^{-/-}$ mice and their littermates. (**G** and **H**) Values are mean ± SD; $n = 4$. *$P < 0.05$.

suggested for rat, boar, and human spermatozoa (22, 23). However, the molecular mechanisms underlying the sperm phospholipid remodeling during epididymal transit still remain unknown.

Phospholipase A_2 (PLA_2) is a group of enzymes that hydrolyze the *sn*-2 position of glycerophospholipids to yield fatty acids (typically unsaturated) and lysophospholipids, which are further converted to a variety of lipid mediators. Of more than 30 mammalian PLA_2-related enzymes identified so far, targeting of 3 genes has been shown to affect reproduction. Ablation of *Pla2g4a* (group IVA cytosolic $PLA_2\alpha$, also known as $cPLA_2\alpha$), impairs multiple steps of female reproduction, because of reduced synthesis of PGs (2, 3), whereas that of *Pla2g6* (group VIA Ca^{2+}-independent PLA_2, also known as $iPLA_2\beta$) and *Pafah1b2* (type I platelet-activating factor acetylhydrolase or group VIIIB PLA_2) results in defective sperm motility and severe impairment of spermatogenesis, respectively, through unknown mechanisms (24, 25). Secreted PLA_2 ($sPLA_2$) enzymes represent a group of structurally related enzymes, with strict Ca^{2+}-dependence and a His-Asp catalytic dyad, and 10 catalytically active $sPLA_2$ enzymes have been identified in mammals (26, 27). Recent studies employing transgenic (gain-of-function) and knockout (loss-of-function) mice have revealed that individual $sPLA_2$s are involved in distinct biological events, such as dietary phospholipid

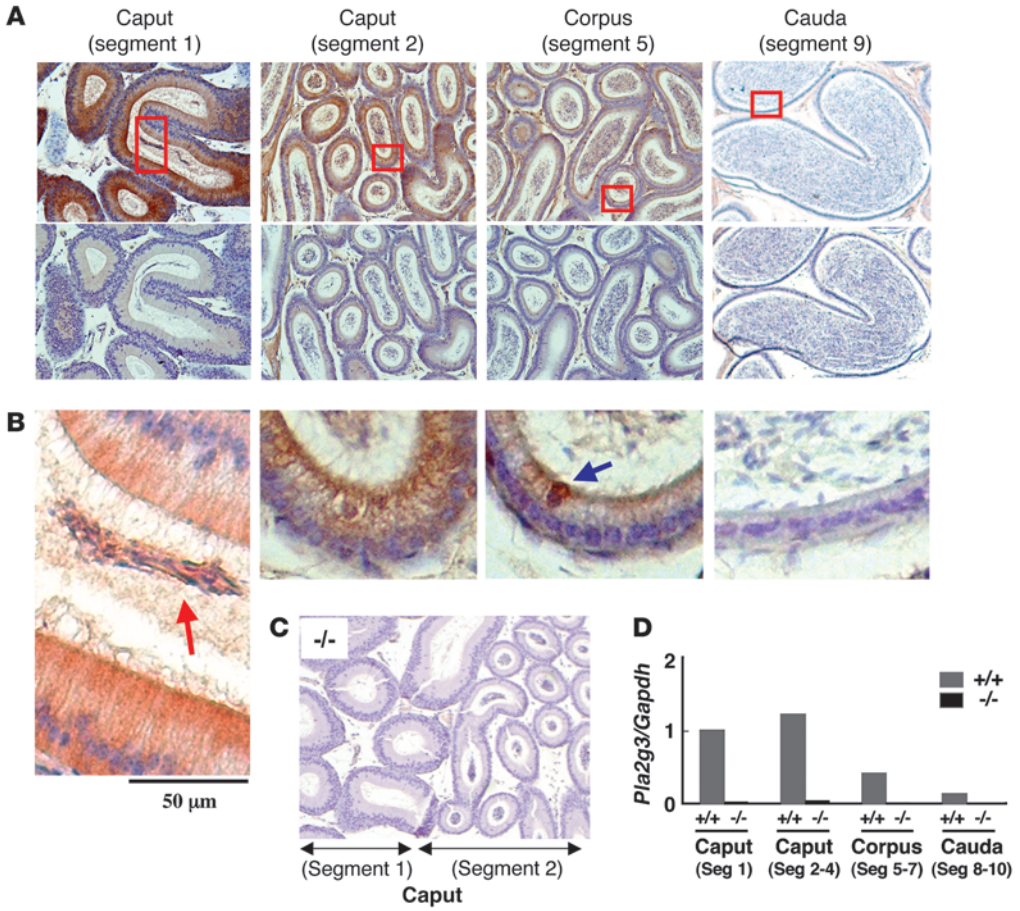

Figure 2
Immunohistochemistry of $sPLA_2$-III in mouse epididymis. (**A**) Serial sections of caput, corpus, and cauda in the epididymis of WT mice were immunostained with anti–$sPLA_2$-III antibody (top panels) or control (preimmune) antibody (bottom panels) (original magnification, ×200). (**B**) High-magnification images of boxed areas of individual sections in **A** are shown. Scale bar: 50 μm. Intense staining of the luminal epithelium in the caput and relatively weak staining of that in corpus were seen as a red-brown color. In the caput, sperm cells in the lumen (red arrow) were positively stained. Apical cells in the corpus epithelium were focally and intensely $sPLA_2$-III positive (blue arrow). (**C**) Epididymis from *Pla2g3*$^{-/-}$ mice was not stained with anti–$sPLA_2$-III antibody (original magnification, ×200). (**D**) Real-time PCR of *Pla2g3* mRNA in different portions of the epididymis from *Pla2g3*$^{+/+}$ and *Pla2g3*$^{-/-}$ mice. The expression level of *Pla2g3* mRNA in the caput segment 1 of *Pla2g3*$^{+/+}$ epididymis was regarded as 1.

digestion (28), host defense (29, 30), inflammation (31, 32), tissue injury (33, 34), and atherosclerosis (35). However, the physiological roles of individual $sPLA_2$s still remain largely obscure.

Group III $sPLA_2$ ($sPLA_2$-III) is distinctive among mammalian $sPLA_2$s, consisting of a central $sPLA_2$ (S) domain flanked by unique N-terminal and C-terminal domains, the S domain being homologous to bee venom PLA_2, rather than to other mammalian $sPLA_2$s (36–38). Transgenic overexpression of human $sPLA_2$-III in mice, in which the enzyme is processed to the S domain–only form, results in accelerated atherosclerosis, following a high-cholesterol diet, through increased hydrolysis of phospholipids in plasma lipoproteins (39) and in systemic inflammation through increased lipid mediator levels (40). In the present study, we show that targeting disruption of the *Pla2g3* gene in mice results in male hypofertility due to impaired sperm maturation in the epididymis. This is the first demonstration to our knowledge that a particular $sPLA_2$ enzyme regulates the process of sperm maturation, likely through control of local lipid homeostasis in the genital tract.

Results

Expression of $sPLA_2$-III in reproductive organs. RT-PCR showed broad expression of *Pla2g3* mRNA in various tissues of C57BL/6 mice, among which the highest level of expression was found in the brain and testis (Figure 1A). Of the male genital organs, *Pla2g3* mRNA was expressed at high levels in the testis and epididymis and to a lesser extent in the seminal vesicles and prostate (Figure 1B, left). In females, more *Pla2g3* transcript was detected in the ovary and oviduct than in the uterus (Figure 1B, right). Immunoblotting of cauda epididymal exudates with anti–$sPLA_2$-III antibody detected an 18-kDa immunoreactive band in epididymal fluid but not in sperm cells (Figure 1C), suggesting that $sPLA_2$-III is secreted into the epididymal duct and is fully processed (38, 39) but is not present in mature sperm.

Generation of Pla2g3 knockout mice. The *Pla2g3*-directed targeting vector, in which the exons encompassing the catalytic domain of the *Pla2g3* gene were replaced with a neomycin resistance cassette (*Neo*^{r}), was constructed (Figure 1D) and transfected into mouse ES cells of 129SvEv origin. Appropriately targeted ES cell clones, as evaluated by

Table 1
Fecundity of *Pla2g3*$^{+/+}$, *Pla2g3*$^{+/-}$, and *Pla2g3*$^{-/-}$ mice

Male genotype	Female genotype	Delivery	Litter size (mean ± SEM)	Total pups (breakdown of pup genotypes)
+/+	+/+	33	8.2 ± 0.4	270 (270 +/+)
+/+	+/–	60	7.4 ± 0.3	446 (217 +/+, 229 +/–)
+/+	–/–	6	6.7 ± 0.7	43 (43 +/–)
+/–	+/+	20	4.4 ± 0.5[A]	87 (45 +/+, 42 +/–)
+/–	+/–	47	2.5 ± 0.5[A]	128 (34 +/+, 65 +/–, 29 –/–)
+/–	–/–	7	3.7 ± 0.8[A]	26 (13 +/–, 13 –/–)
–/–	+/+	13	2.9 ± 1.2[A]	29 (29 +/–)
–/–	+/–	20	4.2 ± 0.6[A]	80 (37 +/–, 43 –/–)
–/–	–/–	22	2.2 ± 0.4[A]	49 (49 –/–)

[A]$P < 0.01$ versus +/+ × +/+.

genomic Southern blotting (Supplemental Figure 1A; supplemental material available online with this article; doi:10.1172/JCI40493DS1), were used to obtain chimeric mice that transmitted the disrupted locus through the germ line. Genotyping was performed on genomic DNA isolated from tail biopsy samples using PCR (Figure 1E), in which 627-bp and 375-bp amplified fragments represented the mutant and WT alleles, respectively. Successful gene ablation of *Pla2g3* was confirmed by the absence of its transcript in the testis and epididymis of *Pla2g3*$^{-/-}$ mice (Figure 1F). Also, the *Pla2g3* mRNA expression was reduced partially in heart, kidney, and liver from *Pla2g3*$^{+/-}$ mice compared with *Pla2g3*$^{+/+}$ mice and was undetectable in *Pla2g3*$^{-/-}$ mice (Supplemental Figure 1B). Two independent ES clones gave rise to mutant mouse lines with virtually identical phenotypes (see below).

PLA_2 enzymatic activity in the cauda epididymal fluid was decreased to approximately 40% in *Pla2g3*$^{-/-}$ mice compared with the activity in *Pla2g3*$^{+/+}$ mice (Figure 1G), indicating that $sPLA_2$-III accounts for nearly half of the total PLA_2 activity in epididymal fluid and that the remaining activity detected in *Pla2g3*$^{-/-}$ mice may be due to the presence of other $sPLA_2$(s) present in the male reproductive organs (41). As shown in Figure 1H, the $sPLA_2$ activity in the fluid of *Pla2g10*$^{-/-}$ mice was reduced by approximately half compared with that of *Pla2g10*$^{+/+}$ mice. These results suggest that $sPLA_2$-III and $sPLA_2$-X are 2 major $sPLA_2$s present in the mouse epididymal fluid. Considering that $sPLA_2$-X is a major $sPLA_2$ isoform residing in sperm acrosomes (41), the $sPLA_2$-X activity in the fluid may reflect a fraction of the enzyme that had been leaked from capacitated spermatozoa during sample preparation.

Immunohistochemical staining of testis sections using anti–$sPLA_2$-III antibody revealed distribution of $sPLA_2$-III in a net-like structure in the seminiferous tubules in WT but not knockout mice (Supplemental Figure 1C), suggesting that $sPLA_2$-III is localized in Sertoli cells rather than in spermatogenic cells. Expression of *Pla2g3* mRNA in Sertoli cells was confirmed using quantitative RT-PCR analysis, in which *Pla2g3* mRNA was enriched in Sertoli cells as compared with the whole testis (Supplemental Figure 1D). In comparison, expression of *Pla2g10* mRNA in Sertoli cells was very low relative to that in the whole testis (Supplemental Figure 1D), in line with the location of $sPLA_2$-X in spermatogenic cells (41). Leydig cells in the interstitium also stained positively for $sPLA_2$-III (Supplemental Figure 1C).

In the epididymis of WT mice, $sPLA_2$-III was intensely expressed in the luminal epithelium of the caput (Figure 2, A and B). Focal staining was also found in principal cells in the corpus of the epididymis, whereas it was barely detectable in the cauda of the epididymis (Figure 2, A and B). The staining was also associated with spermatozoa, luminal space, and luminal cilia on the epithelium in the caput and corpus but not in the cauda (Figure 2B). No such positive staining was detected in the epididymis of *Pla2g3*$^{+/+}$ mice stained with control serum (Figure 2A) or that of *Pla2g3*$^{-/-}$ mice stained with anti–$sPLA_2$-III antibody (Figure 2C). These results, together with the apical border locations within principal and apical cells, suggest that $sPLA_2$-III is secreted apically from the epithelium and associates with luminal sperm cells and cilia in the caput to corpus epididymidis. The faint staining of connective tissue in all regions of the epididymis appeared to be nonspecific, since similar interstitial staining of serial sections was also seen with control antibody. The distribution of $sPLA_2$-III protein in the epididymis of *Pla2g3*$^{+/+}$ mice was consistent with the results of quantitative RT-PCR, which showed higher levels of its mRNA expression in the caput than in the corpus and cauda, whereas *Pla2g3* mRNA was not detected in any place of *Pla2g3*$^{-/-}$ epididymis (Figure 2D). The expression of $sPLA_2$-III in human epididymal epithelium was also verified by immunohistochemical staining (Supplemental Figure 2). Grossly, under light microscopy, the histology of the testis (Supplemental Figure 1C) and epididymis (Figure 2A) of *Pla2g3*$^{-/-}$ mice appeared normal.

Reproduction abnormality in male Pla2g3-deficient mice. During the course of backcrossing (to C57BL/6J mice) and test mating, we found that the litter size after intercrossing heterozygous mutant male and female mice (2.5 ± 0.5 pups per litter) was significantly smaller than that after intercrossing the WT male and female mice (8.2 ± 0.4 pups per litter) (Table 1). Despite this reproductive problem, the ratio of the genotypes of heterozygous male and female offspring exhibited roughly mendelian proportions (*Pla2g3*$^{+/+}$/*Pla2g3*$^{+/-}$/*Pla2g3*$^{-/-}$, 34:65:29, among 128 pups), and the homozygous-null mice were indistinguishable from their WT littermates in terms of survival rates, appearance, and gross behavior, suggesting that the lack of $sPLA_2$-III did not affect embryonic and postnatal development under normal housing conditions. When mutant males were mated with WT females, the litter sizes were reduced in a genotype-related manner, with only 4.4 ± 0.5 and 2.9 ± 1.2 pups per litter after breeding of *Pla2g3*$^{+/-}$ and *Pla2g3*$^{-/-}$ males with *Pla2g3*$^{+/+}$ females (Table 1), respectively, regardless of normal mounting behavior and production of copulatory plugs. In contrast, reduction in the litter size was not evident when mutant females were mated with WT males (Table 1). These results suggest that the loss of $sPLA_2$-III results in male hypofertility. It was noteworthy that, after backcrossing to a C57BL/6J background for several generations, mutant males did not produce any pups, suggesting a genetic influence on the sterile phenotype, as has been demonstrated for several other targeted mutations in sperm (42–45). Therefore, subsequent experiments were conducted using mice with a 129Sv × C57BL/6J mixed background.

Body, testis, and epididymis weights of the mutant mice did not differ from those of their WT counterparts (Supplemental Table 1). Serum testosterone levels were comparable between *Pla2g3*$^{-/-}$ and *Pla2g3*$^{+/+}$ mice (Supplemental Table 1), implying that the reproduction abnormality of *Pla2g3*$^{-/-}$ mice was not caused by

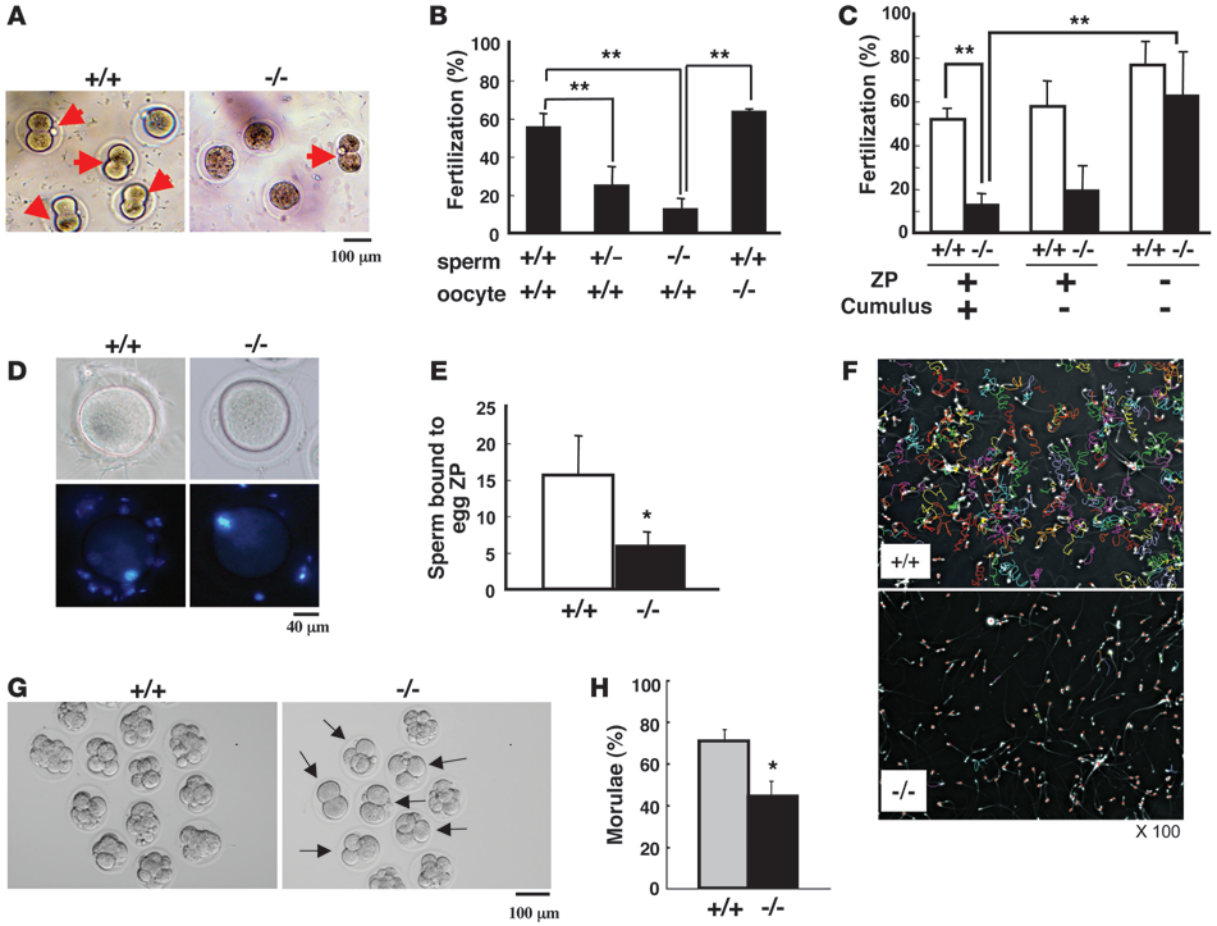

Figure 3

Sperm dysfunction of *Pla2g3*$^{-/-}$ mice. (**A** and **B**) Impaired IVF of *Pla2g3*$^{-/-}$ sperm. (**A**) Representative photos of WT eggs incubated for 24 hours with sperm (200 cells/μl) from *Pla2g3*$^{+/+}$ and *Pla2g3*$^{-/-}$ mice are shown. (**B**) Fertilization efficiency was evaluated as the number of 2-cell stage eggs (arrows in **A**) relative to the total number at 24 hours (mean ± SD; $n = 12$~15; $^{**}P < 0.01$). (**C**) Restored fertilization of *Pla2g3*$^{-/-}$ spermatozoa after removal of the ZP from eggs (mean ± SD; $n = 4$; $^{**}P < 0.01$). (**D** and **E**) Impaired binding of *Pla2g3*$^{-/-}$ sperm to ZP. Sperm from *Pla2g3*$^{+/+}$ and *Pla2g3*$^{-/-}$ mice were incubated for 3 hours with WT eggs, and the nuclei of the sperm bound to the eggs were stained with Hoechst 333412. (**D**) Representative photos of phase-contrast (top panels) and fluorescence (bottom panels) fields are shown. (**E**) The numbers of spermatozoa bound to eggs were counted (mean ± SD; $n = 3$; $^{*}P < 0.05$). (**F**) Impaired motility of *Pla2g3*$^{-/-}$ sperm. Trails of sperm from *Pla2g3*$^{+/+}$ and *Pla2g3*$^{-/-}$ mice were analyzed using a Sperm Motility Analysis System (original magnification, ×100). (**G** and **H**) After insemination with *Pla2g3*$^{+/+}$ and *Pla2g3*$^{-/-}$ sperm, eggs that developed to the 2-cell stage were collected on day 1 and cultured by day 3. (**G**) Arrows indicate eggs whose progression to the morula stage was delayed or stopped. (**H**) The proportion of eggs that developed into morulae relative to those at the 2-cell stage was calculated (mean ± SD; $n = 5$; $^{*}P < 0.05$). Scale bar: 100 μm (**A**, **G**, and **F**); 40 μm (**D**).

imbalance of the gonadal hormone. Although defects in testicular spermatogenesis are often accompanied by the reduction of sperm counts, the numbers of cauda epididymal spermatozoa from both genotypes were similar (Supplemental Table 1), suggesting that germ cell development in the testis was not deeply affected by the lack of sPLA$_2$-III. The testicular (data not shown) and epididymal (Supplemental Figure 3) expressions of other PLA$_2$ enzymes, including *Pla2g4a* (cPLA$_2$α), *Pla2g5* (sPLA$_2$-V), *Pla2g10* (sPLA$_2$-X), *Pla2g6* (iPLA$_2$β), and *Pnpla8* (iPLA$_2$γ), were unaffected by *Pla2g3* deficiency, confirming that the male infertility in *Pla2g3*$^{-/-}$ mice was not due to altered expression of other PLA$_2$s.

Impaired motility and fertility of spermatozoa from Pla2g3-deficient mice. As shown in Figure 3A, sperm from mutant animals showed severely reduced ability to fertilize zona pellucida–intact (ZP-intact) eggs in an in vitro fertilization (IVF) assay. Indeed, epididymal spermatozoa from WT animals fertilized more than 50% of WT eggs at 24 hours after insemination, whereas those from null animals fertilized only approximately 10% of the eggs (Figure 3B). In this experimental setting, spermatozoa from heterozygous mice showed an intermediate reduction of IVF. Accordingly, unfertilized eggs and aborted embryos were increased by the *Pla2g3* deficiency in the IVF assay (Supplemental Figure 4). However, spermatozoa from the mutant mice were able to fertilize eggs normally once the ZP had been removed (Figure 3C). The average numbers of sperm associated with the egg surface was greatly reduced in *Pla2g3*$^{-/-}$ mice, indicating impaired binding of the mutant sperm to the egg ZP (Figure 3, D and E). In contrast, eggs from *Pla2g3*$^{-/-}$ mice underwent normal cell division after incubation with WT sperm (Figure 3A), in line with the normal breeding score of *Pla2g3*$^{-/-}$ females after crossing with *Pla2g3*$^{+/+}$ males (Table 1).

Table 2
Effect of *Pla2g3* deficiency on sperm motility

Sperm parameter	*Pla2g3*$^{+/+}$	*Pla2g3*$^{+/-}$	*Pla2g3*$^{-/-}$
Motile (%)	80.98 ± 3.57	42.91 ± 5.47^{A}	27.37 ± 10.18^{A}
Straight line velocity (μm/s)	45.03 ± 5.04	29.04 ± 2.32^{B}	26.80 ± 1.75^{B}
Curvilinear velocity (μm/s)	166.94 ± 8.86	119.79 ± 7.80^{B}	105.25 ± 9.47^{B}
Amplitude of lateral head displacement (μm)	5.58 ± 0.61	3.66 ± 0.21^{A}	2.95 ± 0.32^{A}
Beat cross frequency (Hz)	14.01 ± 0.48	14.52 ± 0.14	12.90 ± 0.86

The motility of cauda epididymal spermatozoa was analyzed by Sperm Motility Analysis System. Values are mean ± SD (n = 4–7; $^{A}P < 0.01$, $^{B}P < 0.05$ versus *Pla2g3*$^{+/+}$).

We noted that spermatozoa from mutant mice showed impaired motility. The flagellar motion of sperm from *Pla2g3*$^{-/-}$ animals was sluggish and rarely resulted in forward movement. Computer-assisted sperm analysis demonstrated that the sperm tracks differed clearly between the genotypes (Figure 3F and Table 2). Various parameters of sperm motility, including straight-line and curvilinear velocities and amplitude, were markedly reduced in spermatozoa from *Pla2g3*$^{-/-}$ mice (Supplemental Video 1) as compared with those from *Pla2g3*$^{+/+}$ mice (Supplemental Video 2). The motility parameters of spermatozoa from heterozygous mice showed values that were intermediate between those from the WT and null animals (Table 2).

To observe the effect of *Pla2g3* disruption on sperm migration within the female reproductive tract, cross sections of the uterus and oviduct 0.5 days after coitus were prepared. Spermatozoa from *Pla2g3*$^{+/+}$ mice were readily found throughout the uterine tract, and a few sperm cells were present in the oviduct. Although spermatozoa from *Pla2g3*$^{-/-}$ mice accumulated in the lower part of the uterus, they did not reach the upper part of the uterus and the oviduct (Supplemental Figure 5). These results suggest that, because of their impaired forward progression, the mutant sperm failed to swim up through the female genital tract, thereby displaying reduced fertilization efficiency.

We further evaluated the effect of sPLA$_2$-III deficiency on morula development following sperm-egg fusion in vitro. To this end, after WT eggs had been inseminated with *Pla2g3*$^{+/+}$ or *Pla2g3*$^{-/-}$ sperm, those that developed to the 2-cell stage were selected on day 1 and cultured for additional 2 days. In this setting, as expected, morulae were normally recovered from eggs that had fused with the WT sperm, whereas fewer eggs that had fused with the knockout sperm progressed beyond the 2- or 4-cell stage (Figure 3G), thus revealing poor morula development (Figure 3H). Consistently, the reimplanted embryos obtained from *Pla2g3*$^{-/-}$ sperm gave rise to smaller litter size than those from WT sperm (data not shown).

In addition, spermatozoa from *Pla2g3*$^{-/-}$ mice contained a markedly lower level of ATP than those from *Pla2g3*$^{+/+}$ mice, while those from *Pla2g3*$^{+/-}$ mice had an intermediate level (Figure 4A). Probably due to the low level of ATP as well as to defects in other signals, inducible tyrosine phosphorylation of several proteins in spermatozoa that were placed in a capacitating medium, a prerequisite step leading to hyperactivation of flagellar beating (46), was partially, if not completely, reduced in *Pla2g3*$^{-/-}$ mice compared with *Pla2g3*$^{+/+}$ mice (Figure 4, B and C). During sperm maturation, fertilin β, in concert with the molecular chaperone calmegin, is processed from a 100-kDa precursor form present in the testis to a 45-kDa mature form in the epididymis (Figure 4D) (47). An additional approximately 30-kDa immunoreactive band was markedly increased in the epididymis of *Pla2g3*$^{-/-}$ mice compared with that of WT mice (Figure 4D), suggesting unusual fertilin β processing in the knockout epididymis. Since the processing of fertilin β to the 30-kDa species usually takes place after the acrosome reaction (48), the result shown in Figure 4D suggests that the acrosomes of *Pla2g3*-deficient sperm are unstable. Indeed, light microscopic examination showed that, in contrast to the normal appearance (hook-shaped head and straight tail) of *Pla2g3*$^{+/+}$ sperm, *Pla2g3*$^{-/-}$ sperm frequently possessed round-shaped heads (indicative of defective acrosome biogenesis) as well as coiled, bent, or duplicate tails (Figure 4E). When counted, nearly half of the cauda epididymal spermatozoa had abnormal heads in *Pla2g3*$^{-/-}$ mice (Figure 4F) (also see below).

Ultrastructural abnormalities in spermatozoa from Pla2g3-deficient mice. Transmission EM analysis further revealed structural defects in cauda epididymal spermatozoa of *Pla2g3*$^{-/-}$mice. In the axoneme of WT sperm, the outer and inner dynein arms attached to the 9 microtubule doublets that are connected to each other via nexin links (Figure 5A). The axonemal central apparatus consists of 2 microtubules, bridges between the 2, and the central sheath. The radial spokes extend from each doublet, and the radical spoke heads are adjacent to the central sheath. Each axoneme doublet is associated with a dense fiber, and the fibrous sheath has 2 longitudinal columns and regularly spaced ribs. In contrast, *Pla2g3*$^{-/-}$ mice had abnormal sperm with an inappropriate 9 plus 2 configuration of doublets in the flagellar axoneme, in which the most prevalent structural abnormality involved incomplete axonemal doublets, due to loss of one doublet or half of the axonemal complex (Figure 5A). Many of these sperm also lacked the central pair of microtubules and possessed disorganized outer dense fibers. Furthermore, some *Pla2g3*$^{-/-}$ sperm had developed double axonemes in the principal piece and even in the midpiece of the flagellum, where outer dense fibers were mislocated outside the mitochondrial lines (Figure 5B). Such alterations have often been observed in mutant mice harboring (even haploinsufficient) defects in structural proteins for flagellar axonemes (49–53). In addition, the acrosomes of some spermatozoa from *Pla2g3*$^{-/-}$ mice were unusually expanded (Figure 5C), and vacuoles were often found beneath the acrosome cap (Figure 5C). Furthermore, the middle piece of *Pla2g3*$^{-/-}$ spermatozoa appeared disorganized, with unequally sized and swollen mitochondria that had failed to establish the usual regular helical pattern (Figure 5D), which may have some relation to the reduced ATP synthesis, resulting from *Pla2g3* deficiency (Figure 4A). In contrast to the marked ultrastructural abnormalities in cauda spermatozoa, sperm cells with abnormal morphology were scarcely found in the testis and even in the caput epididymidis of *Pla2g3*$^{-/-}$ mice (Figure 5E). Thus, the sperm flagellar malformation in *Pla2g3*$^{-/-}$ mice occurred mainly during epididymal transit from the caput to the cauda (Figure 5F). Although the ultrastructural morphology of epithelial principal cells in the epididymis of *Pla2g3*$^{-/-}$ mice displayed few overt abnormalities, there was a trend toward accumulation of larger cytoplasmic vesicles in the caput epithelium in *Pla2g3*$^{-/-}$ mice when compared with *Pla2g3*$^{+/+}$ mice (Supplemental Figure 6).

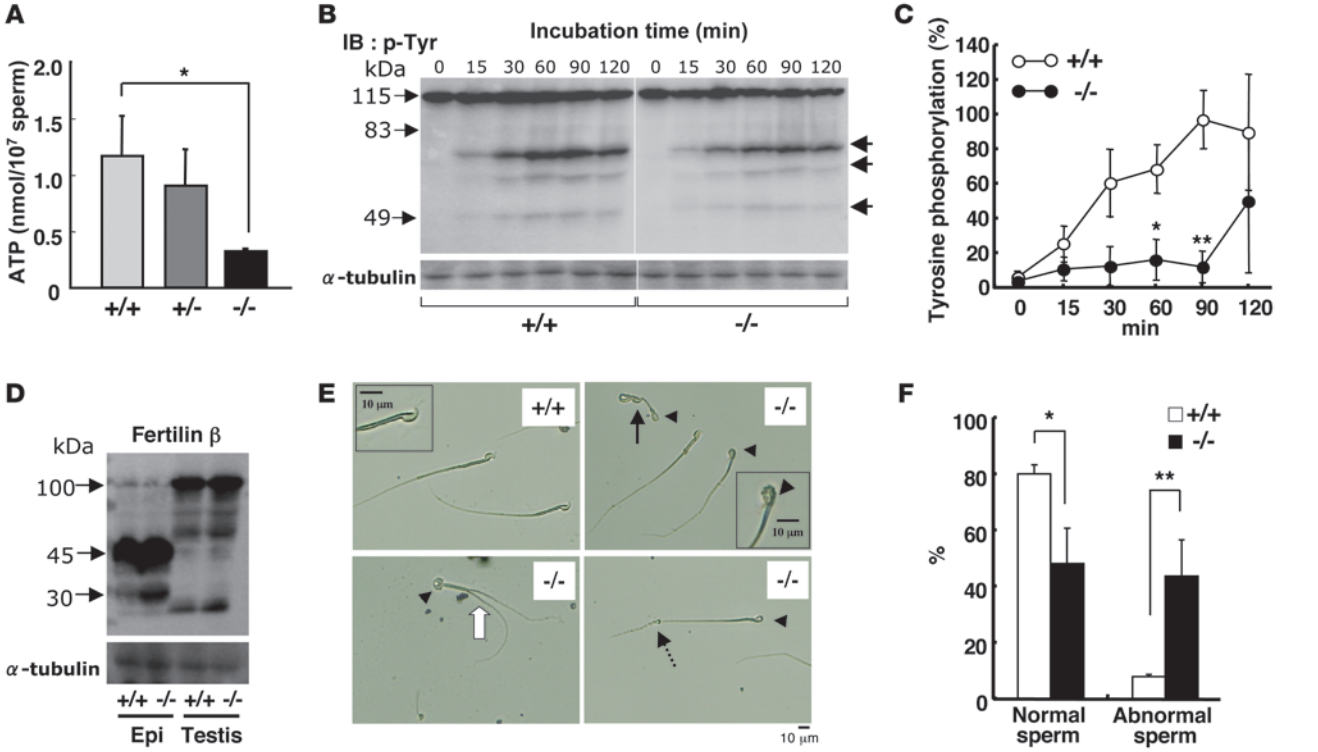

Figure 4
Unusual biochemical properties and morphology of *Pla2g3*$^{-/-}$ sperm. (**A**) ATP contents of capacitated sperm from *Pla2g3*$^{+/+}$, *Pla2g3*$^{+/-}$, and *Pla2g3*$^{-/-}$ mice (mean ± SD; $n = 8$; *$P < 0.05$). (**B** and **C**) Sperm from *Pla2g3*$^{+/+}$ and *Pla2g3*$^{-/-}$ mice were incubated for the indicated periods in HTF medium, and 10^6 sperm cell equivalents were subjected to SDS-PAGE/immunoblotting with anti-phosphotyrosine antibody. (**B**) Arrows on the right margin indicate the bands that were increased during capacitation and reduced in *Pla2g3*$^{-/-}$ mice compared with *Pla2g3*$^{+/+}$ mice, and arrows on the left indicate molecular weight. Blot lanes were run on the same gels but were noncontiguous. (**C**) Inducible phosphorylation of 80-kDa protein relative to constitutive phosphorylation of 115-kDa hexokinase was calculated, with the intensity at 90 minutes being regarded as 100% (mean ± SD; $n = 5$; *$P < 0.05$, **$P < 0.01$). (**D**) Homogenates of testis and epididymis (epi) of *Pla2g3*$^{+/+}$ and *Pla2g3*$^{-/-}$ mice (20 μg protein) were subjected to SDS-PAGE/immunoblotting with anti–fertilin β antibody. Arrows indicate 100-, 45-, and 30-kDa forms. (**E**) Morphology of sperm from *Pla2g3*$^{+/+}$ and *Pla2g3*$^{-/-}$ mice under light microscopy (original magnification, ×200). *Pla2g3*$^{-/-}$ sperm frequently showed a round-shaped head (arrowheads) as well as coiled (filled arrow), bent (dashed arrow), and duplicate (open arrow) tails. Sperm heads are magnified in the insets. Scale bar: 10 μm. (**F**) The proportions of cauda epididymal spermatozoa with or without defects in head morphology were evaluated (mean ± SD; $n = 7$; *$P < 0.05$, **$P < 0.01$).

Altered lipid profiles in the gonads of Pla2g3$^{-/-}$ *mice*. Considering that sPLA$_2$-III is a lipolytic enzyme, it was anticipated that the abnormalities in spermatozoa of *Pla2g3*$^{-/-}$ mice would be caused by alteration of lipid metabolism in the gonads. To address this issue, we performed electrospray ion source/mass spectrometry (ESI-MS) profiling of phosphatidylcholine (PC), a major phospholipid, in spermatozoa from the caput (Figure 6A) and cauda (Figure 6B) epididymidis. Relative abundances of individual PC molecular species, in comparison with the signal intensity of the internal standard PC28:0 (14:0–14:0; m/z = 678), are summarized in Figure 6C. In sperm of *Pla2g3*$^{+/+}$ mice, peaks of PC species with *sn*-2 oleic, linoleic, and arachidonic acids (e.g., PC34:1 [16:0–18:1; m/z = 760], PC36:1 [18:0–18:1; m/z = 788], PC36:2 [18:0–18:2; m/z = 784], PC36:4 [16:0–20:4; m/z = 782], and PC38:4 [18:0–20:4; m/z = 810]) were less abundant in the cauda epididymidis than in the caput epididymidis, whereas those with *sn*-2 DPA and DHA (e.g., PC40:5 [18:0–22:5] and PC40:6 [18:0–22:6]) were higher in the cauda than in the caput (Figure 6C). These results indicate a significant increase in the degree of unsaturation of the fatty acyl components of PC during epididymal transit of sperm, which has been proposed to confer greater flexibility on the sperm membrane and thus higher motility (17–21).

We found that the fatty acyl composition of PC in cauda but not caput epididymal spermatozoa of *Pla2g3*$^{-/-}$ mice differed markedly from that of *Pla2g3*$^{+/+}$ mice (Figure 6, A–C). Although PC species with oleic acid (PC34:1 and PC36:1) in sperm cells were decreased following their transit from the caput or cauda epididymidis in *Pla2g3*$^{+/+}$ mice, this reduction was noticeably compromised in *Pla2g3*$^{-/-}$ mice (Figure 6C). Thus, the ratios of oleate-containing PC to total PC in cauda epididymal spermatozoa from *Pla2g3*$^{+/+}$ and *Pla2g3*$^{-/-}$ mice were 10.1% and 21.3%, respectively, revealing 11% more oleate-containing PC in *Pla2g3*$^{-/-}$ sperm than in *Pla2g3*$^{+/+}$ sperm. Furthermore, although the epididymal transit of sperm from the caput to the cauda was accompanied by marked decreases in PC species with arachidonic acid (PC36:4 and PC38:4) in both genotypes, cauda spermatozoa from *Pla2g3*$^{-/-}$ mice still retained significantly more arachidonate-bearing PC than those from *Pla2g3*$^{+/+}$ mice (Figure 6C).

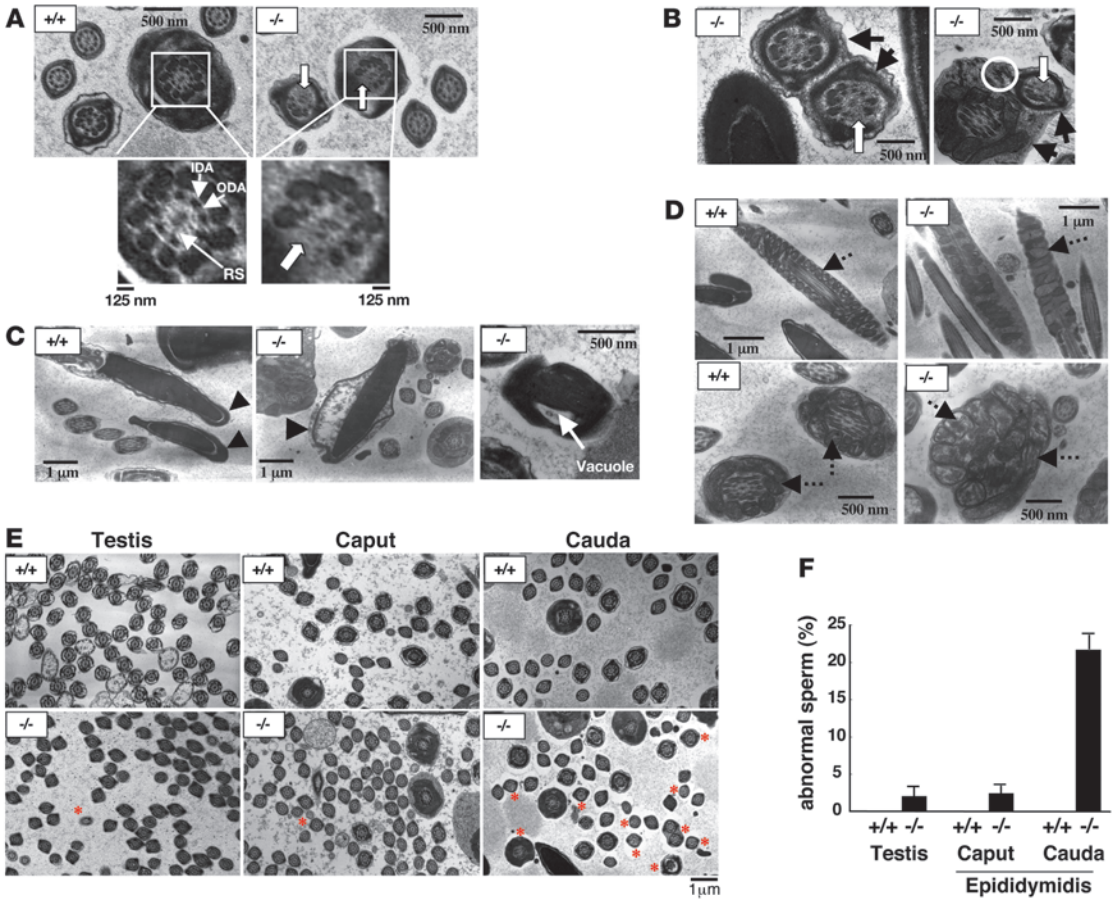

Figure 5

Ultrastructural abnormalities of sperm from *Pla2g3*$^{-/-}$ mice as assessed by transmission EM. (**A**) Transverse sections through the midpiece to principal piece of spermatozoa from *Pla2g3*$^{+/+}$ mice showed the axoneme and axonemal appendages (thin arrows indicate the outer dynein arm [ODA], inner dynein arm [IDA], and radial spoke [RS]) with a 9 plus 2 configuration, whereas those from *Pla2g3*$^{-/-}$ mice often lacked the central pair of microtubules, possessed disorganized outer dense fibers, and showed loss of part or half of the axonemal complex (open arrows). Scale bar: 500 nm (top panel); 125 nm (bottom panel). (**B**) Some sperm from *Pla2g3*$^{-/-}$ mice had double axonemes in the principal piece and even in the midpiece of the flagellum (filled arrows), in which outer dense fibers were mislocated outside the mitochondrial lines (circle). Scale bar: 500 nm. (**C**) In contrast to the well-organized structure of the acrosome in *Pla2g3*$^{+/+}$ sperm, *Pla2g3*$^{-/-}$ sperm had a swollen acrosome (arrowheads) as well as vacuoles beneath the acrosome cap (white arrow). Scale bar: 1 μm (left and center image); 500 nm (right image). (**D**) Longitudinal (top panels) and transverse (bottom panels) sections of the midpiece of *Pla2g3*$^{+/+}$ and *Pla2g3*$^{-/-}$ sperm showed swollen mitochondria in the latter (dashed arrows). Scale bar: 1 μm (top panel); 500 nm (bottom panel). (**E**) Transverse sections of sperm cells in the testis and the caput and cauda epididymidis of *Pla2g3*$^{+/+}$ and *Pla2g3*$^{-/-}$ mice showed that sperm cells with abnormal 9 plus 2 axoneme configuration (red asterisks) were rare in the testis and caput, whereas they were markedly increased in the cauda of the null mice. Scale bar: 1 μm. (**F**) The percentage of spermatozoa with abnormal axonemes in **E** was quantified (mean ± SD; $n = 3$).

PC with linoleic acid (PC36:2) also showed a similar trend. Conversely, increases of PC species with DHA and DPA (PC40:6 and PC40:5) in the cauda epididymidis were less obvious in *Pla2g3*$^{-/-}$ mice than in *Pla2g3*$^{+/+}$ mice (Figure 6C). Accordingly, the ratios of DHA/DPA-containing PC to total PC in cauda epididymal spermatozoa of *Pla2g3*$^{+/+}$ and *Pla2g3*$^{-/-}$ mice were 31.2% and 23.4% (for DHA) and 35.2% and 26.4% (for DPA), respectively, revealing an 8%–9% reduction in DHA/DPA in *Pla2g3*$^{-/-}$ mice relative to *Pla2g3*$^{+/+}$ mice. ESI-MS profiles of PC composition in the sperm-depleted epididymis of the 2 genotypes were nearly identical (Supplemental Figure 7, A and B). These results suggest that sPLA$_2$-III secreted from the epididymal epithelium may act on maturing spermatozoa in the luminal duct in a paracrine manner, thereby facilitating the replacement of fatty acyl chains in PC from ω-6/ω-9 to ω-3 PUFAs in sperm membrane.

Given the aforementioned results, we next investigated whether sPLA$_2$-III would affect the production of some oxygenated metabolites from the arachidonic acid pool released from membrane PC. As assessed by enzyme immunoassay, the levels of PGE_2 and $PGF_{2\alpha}$, which are arachidonate-derived products of the cyclooxygenase pathway, in the epididymal fluid from *Pla2g3*$^{-/-}$ mice were approximately the same as those from *Pla2g3*$^{+/+}$ mice (Supplemental Figure 8A), suggesting that *Pla2g3* deficiency does not affect the production of gonadal prostanoids. To search for other arachidonate metabolites, we performed liquid chromatography electrospray ionization tandem mass spectrometry (LC-ESI-MS/MS) that was optimized for semiquantitative detection of various PUFA-oxygenated products (54, 55). Relative quantities of PUFA metabolites detected thus far in the epididymis of *Pla2g3*$^{-/-}$ mice in comparison

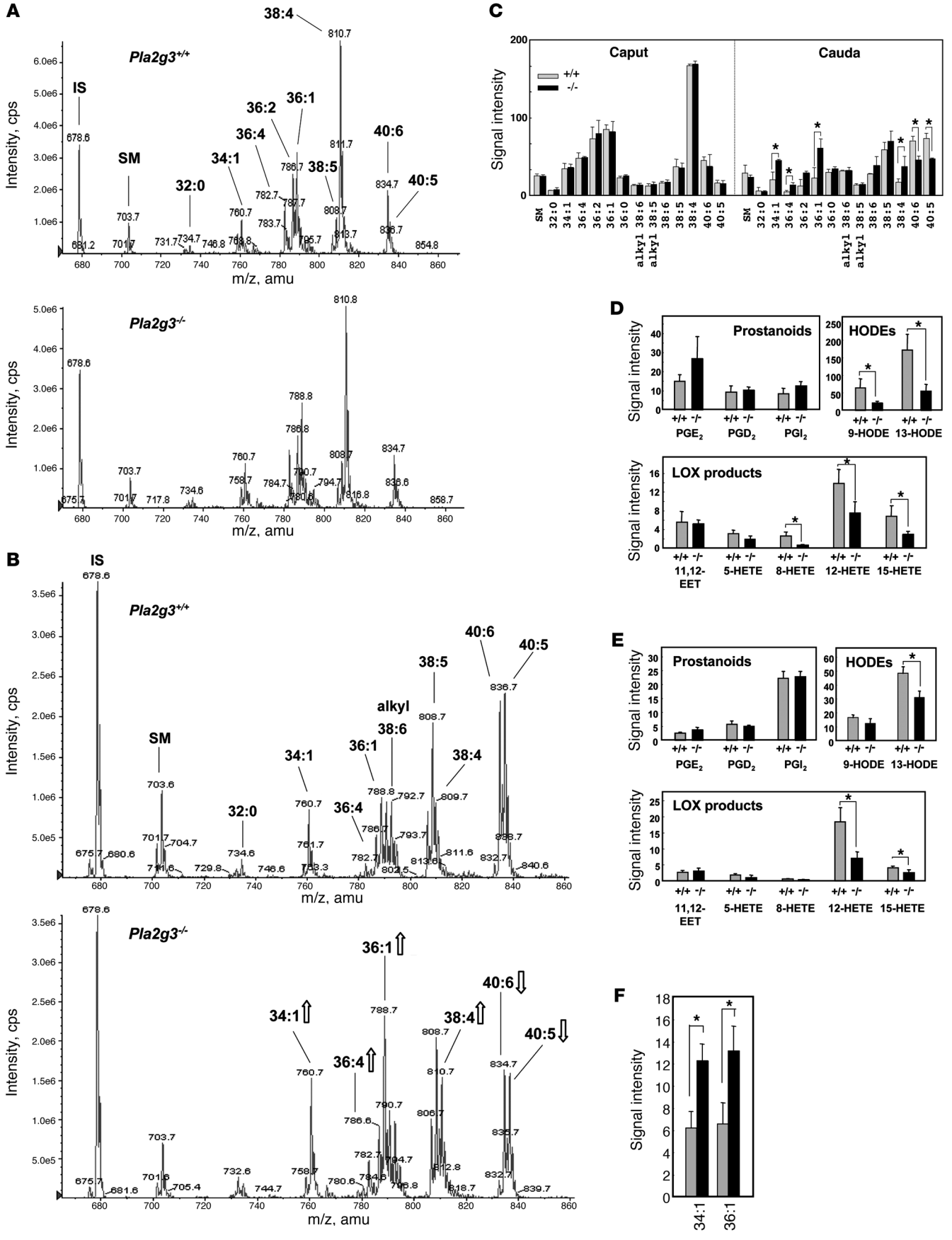
A
Pla2g3+/+
Intensity, cps
m/z, amu
IS
SM
32:0
34:1
36:2
36:4
36:1
38:5
38:4
40:6
40:5
Pla2g3-/-
B
Pla2g3+/+
alkyl
38:6
Pla2g3-/-
C
Caput
Cauda
Signal intensity
+/+
-/-
D
Prostanoids
HODEs
PGE2
PGD2
PGI2
9-HODE
13-HODE
LOX products
11,12-EET
5-HETE
8-HETE
12-HETE
15-HETE
E
F

Figure 6
Altered lipid profiles in the gonads of *Pla2g3*$^{-/-}$ mice. (**A**–**C**) ESI-MS analyses of sperm PC. Representative ESI-MS spectra of PC molecular species in the (**A**) caput and (**B**) cauda epididymal spermatozoa of *Pla2g3*$^{+/+}$ mice and *Pla2g3*$^{-/-}$ mice are shown. IS, internal standard (PC with C28:0; *m*/*z* = 678); SM, sphingomyelin (*m*/*z* = 703). Open arrows in the bottom panel in **B** indicate the peaks for which signal intensities were altered in *Pla2g3*$^{-/-}$ mice in comparison with *Pla2g3*$^{+/+}$ mice. (**C**) PC molecular species determined by ESI-MS in spermatozoa from the caput and cauda epididymidis in *Pla2g3*$^{+/+}$ mice (gray bars) and in *Pla2g3*$^{-/-}$ mice (black bars) are summarized. The relative amounts were expressed as (signal intensity of each peak)/(signal intensity of the internal standard) × 100 (mean ± SD; $n = 3$; $^*P < 0.05$). (**D** and **E**) LC-ESI-MS/MS determination of arachidonate-derived prostanoids, EET and HETEs, and linoleate-derived HODEs in the (**D**) epididymis and (**E**) testis of *Pla2g3*$^{+/+}$ mice (gray bars) and *Pla2g3*$^{-/-}$ mice (black bars). Values represent signal intensities of individual metabolites that were normalized with those of $PGF_{2\alpha}$, which was regarded as 1 (mean ± SD; $n = 5$; $^*P < 0.05$). Using enzyme immunoassay, the level of $PGF_{2\alpha}$ was confirmed to be unchanged as a result of *Pla2g3* deficiency (see text). PGI_2 was evaluated as its stable end product, 6-keto-$PGF_{2\alpha}$. (**F**) PC with oleic acid detected in epididymal fluids from *Pla2g3*$^{+/+}$ mice (gray bars) and *Pla2g3*$^{-/-}$ mice (black bars) (mean ± SD; $n = 3$; $^*P < 0.05$).

with *Pla2g3*$^{+/+}$ mice are summarized in Figure 6D. Consistent with the results of enzyme immunoassay (Supplemental Figure 8A), the levels of PGE_2 as well as other prostanoids, PGD_2 and PGI_2, in both genotypes were indistinguishable (Figure 6D), thus validating the results of LC-ESI-MS/MS. Notably, we found significantly lower levels of several lipoxygenase metabolites, namely 8-hydroxyeicosatetraenoic acid (8-HETE), 12-HETE, and 15-HETE, in the epididymis of *Pla2g3*$^{-/-}$ mice than in that of *Pla2g3*$^{+/+}$ mice (Figure 6D). Moreover, the levels of 9-hydroxyoctadecadienoic acid (9-HODE) and 13-HODE, which are produced from linoleic acid by 12/15-lipoxygenase, were also markedly lower in *Pla2g3*$^{-/-}$ mice than in *Pla2g3*$^{+/+}$ mice (Figure 6D). The levels of 5-HETE and 11,12-epoxyeicosatrienoic acid (11,12-EET), which are arachidonate metabolites of the 5-lipoxygenase and cytochrome P-450 pathways, respectively, did not differ appreciably between the genotypes (Figure 6D). It is notable that a reduction of the 12/15-lipoxygenase products 12- and 15-HETE and 13-HODE, rather than the cyclooxygenase products, was also found in the testis of *Pla2g3*$^{-/-}$ mice compared with *Pla2g3*$^{+/+}$ mice (Figure 6E), even though the compositions of PC molecular species in the testis of the 2 genotypes were similar (Supplemental Figure 7C). The expression level of 12/15-lipoxygenase in the gonads was unaffected by *Pla2g3* deficiency (data not shown). These results collectively suggest that the arachidonic and linoleic acids released by the action of $sPLA_2$-III are coupled with the 12/15-lipoxygenase pathway, in preference to the cyclooxygenase, 5-lipoxygenase, and cytochrome P-450 pathways, in the male reproductive tract of mice. It is unlikely that the selective reduction of 12/15-lipoxygenase products in the gonads of *Pla2g3*$^{-/-}$ mice was due to altered innate immune inflammatory equilibrium, since expression profiles of classical inflammatory cytokines were not altered in the epididymis and testis of the knockout mice (data not shown).

In addition, we found that the epididymal fluid contained substantial levels of PC species with oleic acid (PC34:1 [16:0–18:1] and PC36:1 [18:0–18:1]), which were significantly more abundant in *Pla2g3*$^{-/-}$ mice than in *Pla2g3*$^{+/+}$ mice (Figure 6F). This suggests that the lipid-associated components of epididymal luminal fluid, which appears to include lipoproteins or epididymosomes (microvesicles secreted from epididymal epithelial cells; ref. 17), may be altered in *Pla2g3*$^{-/-}$ mice. Since it has been proposed that PUFAs in the sperm membrane play a protective role against oxidative stress by scavenging reactive oxygen species (18), we assessed the state of lipid peroxidation in the epididymis of *Pla2g3*$^{+/+}$ and *Pla2g3*$^{-/-}$ mice. Although the relative degree of unsaturation of fatty acids in cauda epididymal spermatozoa was lower in *Pla2g3*$^{-/-}$ mice than in *Pla2g3*$^{+/+}$ mice (see above), the level of epididymal lipid peroxidation, as evaluated by accumulation of malondialdehyde and 4-hydroxyalkenals, did not differ significantly between the genotypes (Supplemental Figure 8B).

Discussion

Epithelial cells of the epididymis provide the microenvironment necessary for structural remodeling of spermatozoa (1). Through regulated secretion and reabsorption, they control the pH, osmotic pressure, and composition of epididymal fluids and also the transfer of metabolites such as proteins, sugars, and lipids to and from the sperm surface. Interactions with the proximal epididymis are essential for the acquisition of fertilizing ability by sperm, and alteration of the genes encoding several proteins secreted from the epididymal epithelium often leads to male infertility as a result of defective sperm motility or morphology (10, 42, 56–59). We found that $sPLA_2$-III is expressed in the proximal epididymal epithelium and secreted into the luminal fluid (Figures 1 and 2), that spermatozoa of *Pla2g3*$^{-/-}$ mice are numerically normal but functionally and structurally abnormal (Figures 3–5), and that epididymal sperm of *Pla2g3*$^{-/-}$ mice have an altered phospholipid composition (Figure 6). Importantly, sperm malformation in *Pla2g3*$^{-/-}$ mice proceeds during epididymal transit from the caput to the cauda epididymidis, at which time sperm membrane remodeling is severely impaired, suggesting that the reproductive defect of male *Pla2g3*$^{-/-}$ mice results primarily from altered lipid homeostasis in the epididymis. Our results shed some light on the reported changes in the proportion of DHA and DPA in epididymal maturing sperm in various species, including humans (18–23).

Male but not female *Pla2g3*$^{-/-}$ mice and to a lesser extent *Pla2g3*$^{+/-}$ mice had greatly reduced fertility (Table 1), accompanied by impaired sperm motility (Figure 3F and Supplemental Videos 1 and 2). In agreement, cauda spermatozoa from *Pla2g3*$^{-/-}$ mice had less ATP and lower capacitation-induced tyrosine phosphorylation levels than did those from *Pla2g3*$^{+/+}$ mice (Figure 4, A–C). In addition, cauda spermatozoa from *Pla2g3*$^{-/-}$ mice had aberrant flagellar structures with unusual outer and inner dynein arms, a central pair of microtubules, and a fibrous sheath (Figure 5). In fact, spermatozoa from mice harboring abnormal flagella, due to defects in flagellar axoneme proteins such as Spag6, Spag16, Tekt2, Pacrg, and Akap4, are commonly unable to swim and fail to reach the oviducts in females (49–53), events that are reminiscent of *Pla2g3*$^{-/-}$ mice. Interestingly, flagellar abnormality in *Pla2g3*$^{-/-}$ spermatozoa was less obvious in the testis and caput epididymidis than in the cauda epididymidis (Figure 5, E and F), suggesting that the observed structural changes in *Pla2g3*$^{-/-}$ spermatozoa mainly take place during epididymal transit from the caput to cauda epididymidis. Furthermore, spermatozoa from *Pla2g3*$^{-/-}$ mice showed reduced ability to interact with oocytes (Figure 3, D and E), consistent with abnormal head morphology (globozoospermia) (Figure 4E and Figure 5C). Moreover, even if fertilization was successful, many of the eggs that had fused with

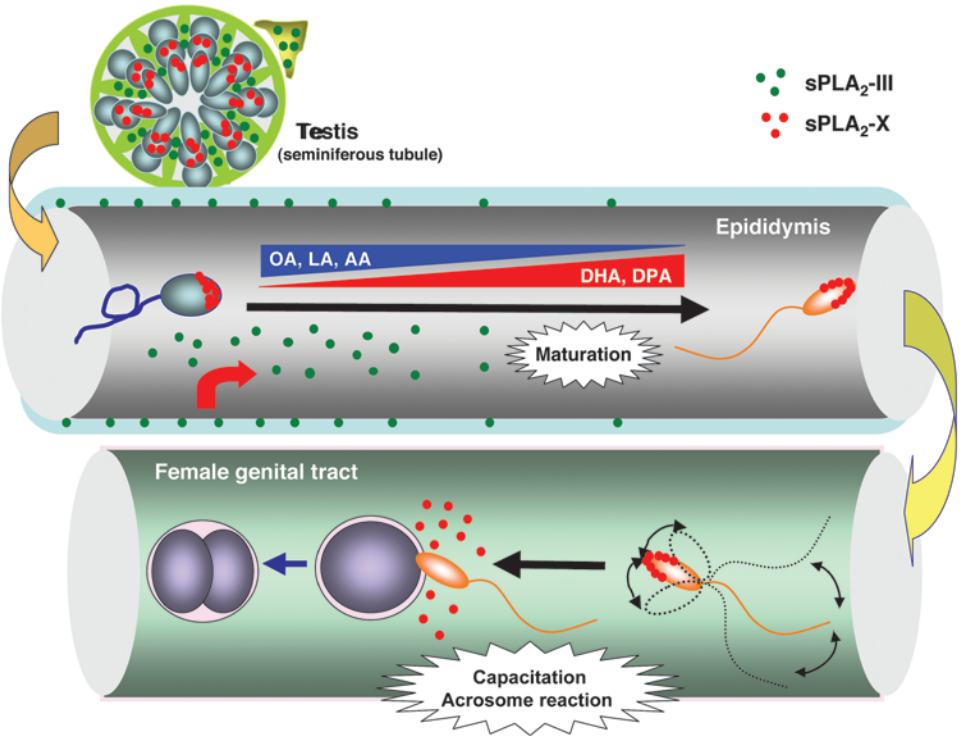

Figure 7
A proposed model for the $sPLA_2$ network in reproduction. During epididymal transit of maturing sperm cells, PC in the sperm membrane undergoes a dramatic remodeling of PUFAs, with more ω-3 and less ω–6/ω–9 PUFAs in mature spermatozoa. $sPLA_2$-III, which is secreted from epithelial cells into the luminal fluid, may regulate this membrane-remodeling process by facilitating deacylation of oleate (OA), linoleate (LA), and arachidonate (AA) from sperm membrane PC. Accordingly, *Pla2g3*$^{-/-}$ sperm contain less DHA/DPA than WT sperm, culminating in abnormal sperm with reduced motility and fertility. Both in the epididymis and testis (in which $sPLA_2$-III is located in supporting cells such as Sertoli cells and Leydig cells), significant portions of the LA and AA liberated by $sPLA_2$-III are metabolized to their oxygenated products by 12/15-lipoxygenase, whose biological significance in sperm maturation remains obscure. $sPLA_2$-III may also regulate lipid transport between spermatozoa and epithelial cells in the epididymis (see text). Another $sPLA_2$ isoform, $sPLA_2$-X, is stored in acrosomes in spermatozoa and is released during capacitation and acrosome reaction to affect fertility (68). Thus, the 2 particular $sPLA_2$s ($sPLA_2$-III and -X), which are expressed in different locations within the male reproductive organs, exert nonredundant functions in 2 major steps of male fertility, one during epididymal sperm maturation and the other during capacitation. Dotted lines indicate sperm movement.

Pla2g3$^{-/-}$ sperm failed to develop properly into morulae (Figure 3, G and H). These results collectively suggest that spermatozoa from *Pla2g3*$^{-/-}$ mice have defects in multiple steps necessary for sperm fertility and even subsequent embryo development, most likely because of impaired sperm maturation.

Sperm cells leaving the testis must pass through the epididymal duct to acquire modifications necessary to reach, recognize, and fuse with the female gamete. Such modifications involve sperm lipid remodeling during interaction of spermatozoa with the epididymal luminal microenvironment, which is loaded with secretions from the epithelial cells (1). The relative abundance of DHA and DPA in mouse spermatozoa has been shown to increase during their passage from the caput to the cauda of the epididymidis, a process that is thought to contribute to increasing the fluidity of the sperm membrane (17), and as a matter of fact, spermatozoa containing higher proportions of DHA have better fertilizing ability in various animal species, including humans (18–23). In the present study, we found that transit of spermatozoa from the caput to the cauda epididymidis was accompanied by decreases in several PC species with oleic, linoleic, and arachidonic acids and by compensatory increases in those with DHA and DPA in the WT sperm membrane, whereas this membrane remodeling was markedly even if not entirely compromised in *Pla2g3*$^{-/-}$ mice (Figure 6, A–C). Accordingly, cauda epididymal spermatozoa in *Pla2g3*$^{-/-}$ mice had PC species containing more oleate and less DHA/DPA than did those in *Pla2g3*$^{+/+}$ mice, a finding that appears to be consistent with previous reports indicating that sperm with higher proportions of DHA have better motility and fertility (17–23). On the basis of these observations, it is tempting to speculate that $sPLA_2$-III may participate in the hydrolysis of PC with oleic, linoleic, and arachidonic acids in the sperm membrane during epididymal transit and that this event may be followed by reacylation of lysophosphatidylcholine, a PLA_2 reaction product, with DHA and DPA, leading to an increase of PC with DPA/DHA in mature sperm. In the *Pla2g3*$^{-/-}$ epididymis, impairment of the deacylation step may eventually perturb the subsequent reconstitution of DPA/DHA in the sperm membrane, culminating in the asthenozoospermia phenotype. The alteration in sperm phospholipid composition in *Pla2g3*$^{-/-}$ mice may not merely affect membrane fluidity required for optimal flagellar motility but may also perturb other membrane-proximal processes required for proper sperm maturation, such as transmembrane signals or protection from oxidative stress (although our data did not support increased lipid peroxidation in the null sperm; Supplemental Figure 8B), in the epididymal niche.

Interestingly, arachidonate/linoleate metabolites of the 12/15-lipoxygenase pathway, but not those of the cyclooxygenase or other eicosanoid pathways, were substantially reduced in the epididymis and even in the testis of *Pla2g3*$^{-/-}$ mice compared with those in *Pla2g3*$^{+/+}$ mice (Figure 6, D and E). To our knowledge, this is the first demonstration that a particular subtype of $sPLA_2$ shows selective functional coupling with a specific arm of the arachidonate-metabolic pathways (in this case, the 12/15-lipoxygenase pathway) in vivo. Given the proposed theory that eicosanoid production is spatiotemporally controlled by sequential biosynthetic enzymes (60, 61), the distinct locations of 12/15-lipoxygenase and cyclooxygenases, respectively, in spermatogenic cells and non-germ

cells (e.g., testicular Sertoli and Leydig cells as well as epididymal epithelial cells) (62, 63) could be regarded as further evidence for the action of $sPLA_2$-III on the sperm membrane, where the arachidonate/linoleate released by $sPLA_2$-III would be more readily accessible to proximal 12/15-lipoxygenase than to distant cyclooxygenases. Although the role of 12/15-lipoxygenase in male fertility has not yet been fully established, expression of this enzyme in spermatogenic cells has led to the suggestion that it may participate in sperm maturation (62). In this context, the possibility that certain 12/15-lipoxygenase–derived lipid mediator(s) may be at least partly responsible for the regulation of sperm maturation by $sPLA_2$-III should be taken into account.

Additionally, $sPLA_2$-III may also affect lipid transport between spermatozoa and epididymal epithelial cells. Several lipoprotein components, such as apoB, apoE, apoA-I, and apoJ (clusterin), are secreted by epididymal epithelial cells (64) and associate with and dissociate from sperm membranes scheduled for endocytosis by epididymal principal cells (65). ApoE receptor-2 and the ABC lipid transporters are abundantly expressed on the epididymal epithelium and sperm membrane, respectively (10, 66). Male fertility can be impaired to various degrees by inactivation of these genes involved in lipoprotein metabolism (8–11). Moreover, membrane transport by epididymosomes, a particular lipoprotein membrane particle emitted from caput epididymal principal cells into the lumen, is fundamental for the process of sperm cell maturation in the epididymis (17, 67). Our speculation that $sPLA_2$-III may also affect this epididymal lipid transport is supported by the finding that the epididymal fluid from *Pla2g3*$^{-/-}$ mice contained more PC than that from *Pla2g3*$^{+/+}$ mice (suggesting impaired hydrolysis of lipoprotein-associated PC) (Figure 6F). Thus, although transgenic overexpression of $sPLA_2$-III in mice leads to systemic hydrolysis of PC in circulating lipoproteins (39), under physiological situations this reaction may operate within a local niche (i.e., the epididymal duct) in which endogenous $sPLA_2$-III is intrinsically expressed.

Although $sPLA_2$-III is expressed in the testis (Figure 1 and Supplemental Figure 1C), our data, including normal sperm counts, testosterone levels and testicular weight, unaltered testicular phospholipid profiles, and minimal alteration in testis histology in *Pla2g3*$^{-/-}$ mice, argue against the significant contribution of this enzyme to testicular spermatogenesis. The only notable alteration in the testis of *Pla2g3*$^{-/-}$ mice is the reduction of 12/15-lipoxygenase products, whose functions in the testis remain obscure in view of the current absence of a report describing the reproductive phenotype in *Alox15*$^{-/-}$ mice. However, our present results do not rule out the possibility that $sPLA_2$-III might participate in certain steps of spermatogenesis or other events in the testis. Considering that several other $sPLA_2$s, including $sPLA_2$-IIC, -IID, -IIF, -V, and -X, are also expressed in distinct cell populations in mouse testis (41), the absence of apparent phenotypes in the testis of *Pla2g3*$^{-/-}$ mice might be because of the redundant or compensatory actions of other $sPLA_2$s in this tissue.

Targeted disruption of *Pla2g6*, which encodes $iPLA_2\beta$, leads to male infertility because of impaired sperm motility (24), and ablation of *Pla2g4a* ($cPLA_2\alpha$), which plays a pivotal role in eicosanoid generation in various biological events, impairs female reproductive ability by preventing implantation and parturition (2, 3). However, despite the fact that various $sPLA_2$s are expressed in male genital organs (41), little has been known about their roles in reproduction. The present work demonstrates for the first time to our knowledge that $sPLA_2$-III, an atypical $sPLA_2$ that is supplied from gonadal microenvironments, controls sperm maturation. In addition, Escoffier et al., in collaboration with us, have very recently shown that $sPLA_2$-X, a sperm acrosomal $sPLA_2$, controls capacitation, acrosome reaction, and thereby fertility (68). Thus, various forms of intracellular and extracellular PLA_2 enzymes participate in the regulation of distinct steps of reproduction through distinct mechanisms. Of particular importance, the sequential control of epididymal sperm maturation and postepididymal sperm capacitation by $sPLA_2$-III from supporting cells and $sPLA_2$-X from sperm acrosomes, respectively, in the gonadal niche has opened new insights into the physiological role of this particular extracellular phospholipase family in the reproduction biology (Figure 7).

Finally, given the fact that $sPLA_2$-III is expressed in human epididymal epithelium (Supplemental Figure 2), it is likely that the enzyme plays a similar role in humans. In this context, the question of whether $sPLA_2$-III might also contribute to the regulation of epididymal sperm maturation in humans needs further elucidation. From a clinical standpoint, the reduced motility and fertilization competence of spermatozoa from male *Pla2g3*-null mice suggest that $sPLA_2$-III is a potential target for the development of male contraceptive agents or a potential diagnosing marker for the male sterility. On the other hand, application of a particular agent that is capable of inhibiting $sPLA_2$-III in patients with atherosclerosis or inflammation might necessitate caution, in light of the associated risk of inducing male infertility.

Methods

Targeted disruption of the Pla2g3 gene. The *pla2g3*-targeting vector was constructed with a *neo*^{r} gene driven by the polyoma enhancer/herpes simplex virus thymidine kinase (MC1) promoter. The MC1-*neo*^{r} cassette was inserted into the exons encompassing the catalytic domain and introns of the *Pla2g3* gene (Figure 1C). The 5.5-kb long arm and 1.7-kb short arm genomic fragments from the *Pla2g3* gene were isolated from the 129SvEv genome using PCR. The diphtheria toxin A gene (*crdta*, a synthetic construct modified diphtheria toxin fragment gene) was inserted at the 3′ end of the short arm of the targeting vector for negative selection. The targeting vector linearized by *Hind*III digestion was transfected into mouse ES cells of 129SvEv origin (Dainippon Sumitomo Pharma). Appropriately targeted ES cell clones were used to obtain chimeric mice that transmitted the disrupted locus through the germ line. The 10- to 15-week-old mice were backcrossed to the C57BL/6J background for 1 or 2 generations; WT littermates were used as controls. Genotyping was performed on genomic DNA isolated from tail biopsies by PCR using the following primers: 5′-TGAGTCAGCTCTCAGGAAGACAAGTCC-3′ (WT forward), 5′-CCATCTTGTTCAATGGCCGATCCCA-3′ (mutant reverse), and 5′-GTGAGAGATGGTGTGGAAGCGGAAA-3′ (WT reverse). The primer set of WT forward and mutant reverse amplified a 627-bp fragment specific for the mutant allele, and the set of WT forward and WT reverse yielded a 375-bp fragment specific for the WT allele. The reaction was carried out using an ExTaq Kit (Takara Bio) with 35 cycles of amplification (95°C for 20 seconds, 60°C for 20 seconds, and 72°C for 30 seconds). For Southern blot analysis, genomic DNA was digested with *Sph*I and hybridized with a probe as indicated in Figure 1C.

Mice lacking $sPLA_2$-X (*Pla2g10*$^{-/-}$) are described elsewhere (68). All mice were housed in climate-controlled (21°C), specific pathogen–free facilities with a 12-hour-light/12-hour-dark cycle, with free access to standard laboratory food (Picolab mouse diet 20; Laboratory Diet) and water. All procedures involving animals were performed in accordance with protocols approved by the Institutional Animal Care and Use Committees of Showa University and of the Tokyo Metropolitan Institute of Medical Science, in accordance with the standards relating to the care and management of experimental animals in Japan.

Histological analyses. Immunohistochemistry of tissue sections was performed as described previously (38, 39). In brief, paraffin-embedded mouse testis and epididymis sections (4-μm thick) were incubated with Target Retrieva Solution (Dako Cytomation) and then with anti–sPLA$_2$-III or control antibody at 1:100 dilution in 10 mM Tris-HCl (pH 7.4), containing 0.15 M NaCl overnight at 4°C. The sections were then treated with a CSA System Staining Kit (Dako Cytomation) with diaminobenzidine substrate, followed by counterstaining with hematoxylin. Human epididymal sections (male, 16 years old) were obtained through surgery at Toho University School of Medicine, following approval by the ethical committee of the Faculty and informed consent from the patient.

For transmission EM, testis and epididymis samples were fixed with 2.5% glutaraldehyde, post-fixed with 2% OsO_4, dehydrated through an ascending ethanol series, passed through propylene oxide, and then embedded in Quetol812 resin (Nisshin EM). Ultrathin sections (90-nm thick) on mesh grids were stained with uranyl acetate and lead acetate and examined with an H-300 electron microscope (Hitachi).

Real-time quantitative RT-PCR. First-strand cDNA synthesis was performed using a High Capacity cDNA Reverse Transcription Kit (Applied Biosystems). Quantitative RT-PCR analysis was carried out on an ABI Prism 7000 Sequence Detection System (Applied Biosystems), using Power SYBR Green PCR Master Mix (Applied Biosystems). For the detection of PLA$_2$ mRNAs, TaqMan probes from Applied Biosystems were used: Mm00555594_m1 and Mm01191142_m1 (*Pla2g3*), Mm00448161_m1 (*Pla2g5*), Mm00449530_m1 (*Pla2g10*), Mm00447040_m1 (*Pla2g4a*), Mm00479527_m1 (*Pla2g6*), and Mm00470656_m1 (*Pnpla8*). The Taqman probe X00686 (*Rn18S*; 18S ribosomal RNA) was used as a control. The thermal cycling conditions comprised an initial denaturation step at 50°C for 2 minutes and 95°C for 10 minutes, followed by 40 cycles of amplification at 95°C for 20 seconds, 55°C for 20 seconds, and 72°C for 30 seconds. Semiquantitative RT-PCR for mouse *Pla2g3* mRNA was performed with a set of primers (5′-GGCTGAGGCCACCTCATATACTTC-3′ and 5′-TCCTTTGCCCTCAGCACAGTCAAG-3′), using ExTaq polymerase with 35 cycles of amplification (95°C for 20 seconds, 60°C for 20 seconds, and 72°C for 30 seconds). The amplified product was electrophoresed on 1% (w/v) agarose gel, with ethidium bromide.

Measurement of PLA$_2$ activity. PLA$_2$ activity was assayed by measuring the amounts of radiolabeled linoleic acid released from the substrate 1-palmitoyl-2-[^{14}C]linoleoyl-phosphatidylethanolamine (Perkin-Elmer), as described previously (37). Each reaction mixture consisted of appropriate amounts of the epididymal fluid, 100 mM Tris-HCl (pH 7.4), 4 mM $CaCl_2$, and the substrate at 1 μM. After incubation for 30 minutes at 37°C, [^{14}C]linoleic acid was extracted, and the radioactivity was quantified with a liquid scintillation counter.

Sperm motility. Male mice (8 weeks old) were sacrificed by cervical dislocation, and a tubule segment was dissected from the cauda epididymidis. The luminal sperm were allowed to disperse in 200 μl of HTF medium (ARK Resource) for 10 minutes. After the tissue had been removed, the sperm were allowed to capacitate for 2 hours at 37°C in 5% CO_2 in air. A 5-μl aliquot of the sperm suspension was then placed in a counting chamber (Standard Count; Laje) for assessment of motility by computer-assisted analysis, using a Sperm Motility Analysis System (KAGA Electronics). The parameters measured were the percentage of motile sperm cells, vigor of movement (curvilinear velocity), speed of forward progression (straight-line velocity), amplitude of lateral head displacement, beat cross-frequency, and linearity of swim path.

IVF. Female mice (10 weeks old) were injected intraperitoneally with 7.5 IU pregnant mare serum gonadotropin (Asuka Pharmacy), followed 48 hours later with 7.5 IU human chorionic gonadotropin (Asuka Pharmacy). Oviducts were collected 13 hours later, and the oocyte cumulus complexes were placed in 100 μl HTF medium in a 60-mm culture dish (Iwaki), and droplets were covered by embryo-tested mineral oil (Nakarai Tesque). As required, oocytes were treated with 0.1% hyaluronidase (Sigma-Aldrich) for 30 minutes at 37°C to remove the cumulus mass, soaked in Tyrode's buffer (Sigma-Aldrich) to remove the ZP, and resuspended in 100 μl HTF medium. Spermatozoa collected from the cauda epididymidis were allowed to swim into 50 μl HTF medium, aspirated, incubated in 200 μl of HTF medium for 60 minutes at 37°C to permit capacitation, diluted, and added to oocyte droplets to achieve a concentration of 200 spermatozoa/μl. After the spermatozoa and oocytes had been coincubated for 6 hours at 37°C, the oocytes were washed and cultured for 24 hours before examination of oocyte fertilization, as demonstrated by the presence of a second polar body and 2 pronuclei, one near a sperm tail.

Sperm binding to the ZP. Cumulus-free oocytes were incubated with spermatozoa (200 cells/μl) in HTF drops for 3 hours at 37°C. After washing, nuclear DNA in the sperm-oocyte complexes was stained with 1 μg/ml Hoechst 33342 (Sigma-Aldrich), and the number of sperm bound to the oocytes was counted using a BZ-9000 fluorescence microscope (Keyence).

Quantification of ATP content of spermatozoa. Cauda epididymal spermatozoa were incubated for 1 hour at 37°C under a 5% CO_2 atmosphere in M16 medium (Sigma-Aldrich). Floating sperm cells (10^7 cells) were collected and resuspended in 50 μl M16 medium, to which 450 μl sample buffer (4 mM EDTA/0.1 M Tris-HCl, pH 7.8) was added, and boiled for 2 minutes. After centrifugation for 5 minutes at 20,000 *g*, ATP in the supernatants was quantified by an ATP Bioluminescence Assay Kit CLS II (Roche Applied Science) and Gene LIGHT 55 (Microtec Nichion).

Immunoblotting. Homogenates of testis and epididymis (20 μg protein equivalents) or cauda epididymal sperm (10^6 cell equivalents) were subjected to SDS-PAGE and transfer to nitrocellulose membranes (Schleicher & Schuell). After blocking, the membranes were incubated with anti–sPLA$_2$-III antibody (a gift from S. Hatakeyama, NOVARTIS Pharma, Tsukuba, Japan, which reacts specifically with sPLA$_2$-III but not with other sPLA$_2$s) (38, 39), anti-ADAM2 (fertilin β) antibody (clone 9D2.2) (Chemicon), anti-phosphotyrosine antibody (PY20) (Santa Cruz Biotechnology Inc.), or anti–α-tubulin antibody (Santa Cruz Biotechnology Inc.) (1:5,000 dilution) and then with horseradish peroxidase–conjugated anti-IgG antibody (Zymed) (1:10,000 dilution) in Can Get Signal Solution (TOYOBO). After washing with TBS-Tween, the membranes were soaked using an ECL Western Blot Analysis System (Amersham) and examined with a Light-Capture Cooled CCD Camera System (ATTO).

Mass spectrometric analysis. Lipids were extracted from tissue or cell homogenates or fluids using the method of Bligh and Dyer (69). Before lipid extraction, PC with C28:0 (14:0–14:0) was added to each sample as an internal standard (2 nmol per epididymal [50 mg] or testicular [200 mg] tissue or whole sperm cells). The ESI-MS analysis was performed using a 4000Q-TRAP quadrupole-linear ion trap hybrid mass spectrometer (Applied Biosystems/MDS Sciex), with an Ultimate 3000 HPLC system (DIONEX) combined with an HTC PAL autosampler (CTC Analytics). The extracted lipids were subjected to ESI-MS analysis by flow injection (3 nmol phosphorus equivalent), with a mobile phase composition of acetonitrile/methanol/water (6:7:2, v/v/v), plus 0.1% ammonium formate, pH 6.8, at a flow rate of 10 μl/min. The scan range of the instrument was set at 200–1,000 m/z, at a scan speed of 1,000 Da/s in the positive ion mode. The trap fill time was set at 1 ms, the ion spray voltage was set at 5,500 V, and the declustering potential was set at 100 V. Nitrogen was used as the curtain gas (setting of 10 arbitrary units) and as the collision gas (set to "high"). The method used for detection of the proper precursor ions and neutral losses derived from phospholipids in ESI-MS/MS analysis has been described previously (70, 71).

For the assay of oxygenated lipids using LC-ESI-MS/MS analysis, tissues were soaked in 10 volumes of methanol and then homogenized with a Polytron homogenizer. After overnight incubation at –20°C, H_2O

was added to the mixture for a final methanol concentration of 10%. *d8*-Labeled arachidonic acid (Cayman Chemicals) was added as an internal standard. The oxygenated lipids in the supernatant were extracted using Sep-Pak C18 cartridges (Waters). The LC-ESI-MS/MS analysis was performed using a 4000Q-TRAP quadrupole-linear ion trap hybrid mass spectrometer (Applied Biosystems/MDS Sciex) with ACQUITY Ultra Performance LC (Waters). The sample was applied to the ACQUITY UPLC BEH C18 column (1 × 150 mm i.d., 0.17 μm particle) and then to ESI-MS/MS analysis. The samples injected by the autosampler (10 μl) were directly introduced and separated by a step gradient with mobile phase A (water containing 0.1% formic acid) and mobile phase B (acetonitrile/methanol, 4:1, v/v) at a flow rate of 50 μl/min and a column temperature of 30°C. The specific detection of individual lipids was performed by multiple reaction monitoring (54, 55).

Other procedures. Levels of serum testosterone and epididymal prostanoids were quantified using respective enzyme immunoassay kits (Cayman Chemicals). Lipid peroxidation was evaluated by quantifying malondialdehyde and 4-hydroxyalkenals, using an LPO Assay Kit BIOXYTECH LPO-586 (OXIS International). Protein concentrations were determined using a BCA protein assay kit (Pierce). The immortalized mouse Sertoli cell line Sertoli B was provided by T. Hara (Tokyo Metropolitan Institute of Medical Science) (72). Data were statistically evaluated by unpaired Student's *t* test, and *P* values of less than 0.05 were considered significant.

Acknowledgments

This work was supported by grants-in aid for Scientific Research (to S. Hara, I. Kudo, and M. Murakami), for Young Scientists (to Y. Taketomi, K. Yamamoto, and H. Sato), and for the High-Tech Research Center Project for Private Universities (matching fund subsidy 2004–2007) (to S. Hara and I. Kudo) from the Ministry of Education, Culture, Sports, Science and Technology of Japan and by grants from PRESTO of the Japan Science and Technology Agency, the NOVARTIS Foundation for the Promotion of Science, and the Toray Science Foundation (to M. Murakami). We would like to thank T. Hara (Tokyo Metropolitan Institute of Medical Science) for providing us the immortalized mouse Sertoli cell line Sertoli-B (72), S. Hatakeyama (NOVARTIS Pharma, Tsukuba, Japan) for providing anti–sPLA$_2$-III antibody (39), and G. Lambeau and C. Arnoult for their helpful discussions.

Received for publication July 13, 2009, and accepted in revised form February 10, 2010.

Address correspondence to: Makoto Murakami, Biomembrane Signaling Project, The Tokyo Metropolitan Institute of Medical Science, 2-1-6 Kamikitazawa, Setagaya-ku, Tokyo 156-8506, Japan. Phone: 81.3.5316.3228; Fax: 81.3.5316.3125; E-mail: murakami-mk@igakuken.or.jp.

1. Cooper TG. Role of the epididymis in mediating changes in the male gamete during maturation. *Adv Exp Med Biol*. 1995;377:87–101.
2. Uozumi N, et al. Role of cytosolic phospholipase A_2 in allergic response and parturition. *Nature*. 1997;390(6660):618–622.
3. Song H, et al. Cytosolic phospholipase A_2alpha is crucial for 'on-time' embryo implantation that directs subsequent development. *Development*. 2002; 129(12):2879–2889.
4. Lim H, et al. Multiple female reproductive failures in cyclooxygenase 2-deficient mice. *Cell*. 1997;91(2):197–208.
5. Hizaki H, et al. Abortive expansion of the cumulus and impaired fertility in mice lacking the prostaglandin E receptor subtype EP_2. *Proc Natl Acad Sci U S A*. 1999;96(18):10501–10506.
6. Ye X, et al. LPA3-mediated lysophosphatidic acid signalling in embryo implantation and spacing. *Nature*. 2005;435(7038):104–108.
7. Fukami K, et al. Requirement of phospholipase Cdelta4 for the zona pellucida-induced acrosome reaction. *Science*. 2001;292(5518):920–923.
8. Huang LS, Voyiaziakis E, Chen HL, Rubin EM, Gordon JW. A novel functional role for apolipoprotein B in male infertility in heterozygous apolipoprotein B knockout mice. *Proc Natl Acad Sci U S A*. 1996; 93(20):10903–10907.
9. Moghadasian MH, Nguyen LB, Shefer S, McManus BM, Frohlich JJ. Histologic, hematologic, and biochemical characteristics of apo E-deficient mice: effects of dietary cholesterol and phytosterols. *Lab Invest*. 1999;79(3):355–364.
10. Andersen OM, et al. Essential role of the apolipoprotein E receptor-2 in sperm development. *J Biol Chem*. 2003;278(26):23989–23995.
11. Selva DM, et al. The ATP-binding cassette transporter 1 mediates lipid efflux from Sertoli cells and influences male fertility. *J Lipid Res*. 2004; 45(6):1040–1050.
12. Flesch FM, Gadella BM. Dynamics of the mammalian sperm plasma membrane in the process of fertilization. *Biochim Biophys Acta*. 2000;1469(3):197–235.
13. Stoffel W, et al. Delta6-desaturase (FADS2) deficiency unveils the role of omega3- and omega6-polyunsaturated fatty acids. *EMBO J*. 2008;27(17):2281–2292.
14. Jung A, Hollmann M, Schäfer MA. The fatty acid elongase NOA is necessary for viability and has a somatic role in *Drosophila* sperm development. *J Cell Sci*. 2007;120(Pt 16):2924–2934.
15. Kubagawa HM, et al. Oocyte signals derived from polyunsaturated fatty acids control sperm recruitment in vivo. *Nat Cell Biol*. 2006;8(10):1143–1148.
16. Ollero M, et al. Characterization of subsets of human spermatozoa at different stages of maturation: implications in the diagnosis and treatment of male infertility. *Hum Reprod*. 2001;16(9):1912–1921.
17. Rejraji H, et al. Lipid remodeling of murine epididymosomes and spermatozoa during epididymal maturation. *Biol Reprod*. 2006;74(6):1104–1113.
18. Lenzi A, Picardo M, Gandini L, Dondero F. Lipids of the sperm plasma membrane: from polyunsaturated fatty acids considered as markers of sperm function to possible scavenger therapy. *Hum Reprod Update*. 1996;2(3):246–256.
19. Lenzi A, et al. Fatty acid composition of spermatozoa and immature germ cells. *Mol Hum Reprod*. 2000;6(3):226–231.
20. Furimsky A, et al. Percoll gradient-centrifuged capacitated mouse sperm have increased fertilizing ability and higher contents of sulfogalactosylglycerolipid and docosahexaenoic acid-containing phosphatidylcholine compared to washed capacitated mouse sperm. *Biol Reprod*. 2005; 72(3):574–583.
21. Aksoy Y, Aksoy H, Altinkaynak K, Aydin HR, Ozkan A. Sperm fatty acid composition in subfertile men. *Prostaglandins Leukot Essent Fatty Acids*. 2006;75(2):75–79.
22. Hall JC, Hadley J, Doman T. Correlation between changes in rat sperm membrane lipids, protein, and the membrane physical state during epididymal maturation. *J Androl*. 1991;12(1):76–87.
23. Haidl G, Opper C. Changes in lipids and membrane anisotropy in human spermatozoa during epididymal maturation. *Hum Reprod*. 1997;12(12):2720–2723.
24. Bao S, et al. Male mice that do not express group VIA phospholipase A_2 produce spermatozoa with impaired motility and have greatly reduced fertility. *J Biol Chem*. 2004;279(37):38194–38200.
25. Koizumi H, et al. Targeted disruption of intracellular type I platelet activating factor-acetylhydrolase catalytic subunits causes severe impairment in spermatogenesis. *J Biol Chem*. 2003;278(14):12489–12494.
26. Kudo I, Murakami M. Phospholipase A_2 enzymes. *Prostaglandins Other Lipid Mediat*. 2002;68–69:3–58.
27. Lambeau G, Gelb MH. Biochemistry and physiology of mammalian secreted phospholipases A_2. *Annu Rev Biochem*. 2008;77:495–520.
28. Labonté ED, Kirby RJ, Schildmeyer NM, Cannon AM, Huggins KW, Hui DY. Group 1B phospholipase A_2-mediated lysophospholipid absorption directly contributes to postprandial hyperglycemia. *Diabetes*. 2006;55(4):935–941.
29. Laine VJ, Grass DS, Nevalainen TJ. Protection by group II phospholipase A_2 against *Staphylococcus aureus*. *J Immunol*. 1999;162(12):7402–7408.
30. Balestrieri B, Maekawa A, Xing W, Gelb MH, Katz HR, Arm JP. Group V secretory phospholipase A_2 modulates phagosome maturation and regulates the innate immune response against *Candida albicans*. *J Immunol*. 2009;182(8):4891–4898.
31. Muñoz NM, Meliton AY, Arm JP, Bonventre JV, Cho W, Leff AR. Deletion of secretory group V phospholipase A_2 attenuates cell migration and airway hyperresponsiveness in immunosensitized mice. *J Immunol*. 2007;179(7):4800–4807.
32. Henderson WR Jr, et al. Importance of group X-secreted phospholipase A_2 in allergen-induced airway inflammation and remodeling in a mouse asthma model. *J Exp Med*. 2007;204(4):865–877.
33. Fujioka D, et al. Reduction in myocardial ischemia/reperfusion injury in group X secretory phospholipase A_2-deficient mice. *Circulation*. 2008; 117(23):2977–2985.
34. Ohtsuki M, et al. Transgenic expression of group V, but not group X, secreted phospholipase A_2 in mice leads to neonatal lethality because of lung dysfunction. *J Biol Chem*. 2006;281(47):36420–36433.
35. Bostrom MA, et al. Group V secretory phospholipase A_2 promotes atherosclerosis: evidence from genetically altered mice. *Arterioscler Thromb Vasc Biol*. 2007;27(3):600–606.
36. Valentin E, Ghomashchi F, Gelb MH, Lazdunski M, Lambeau G. Novel human secreted phospholipase A_2 with homology to the group III bee venom enzyme. *J Biol Chem*. 2000;275(11):7492–7496.
37. Murakami M, et al. Cellular arachidonate-releas-

ing function of novel classes of secretory phospholipase A_2s (groups III and XII). *J Biol Chem*. 2003; 278(12):10657–10667.
38. Murakami M, Masuda S, Shimbara S, Ishikawa Y, Ishii T, Kudo I. Cellular distribution, post-translational modification, and tumorigenic potential of human group III secreted phospholipase A_2. *J Biol Chem*. 2005;280(26):24987–24998.
39. Sato H, et al. Analyses of group III secreted phospholipase A_2 transgenic mice reveal potential participation of this enzyme in plasma lipoprotein modification, macrophage foam cell formation, and atherosclerosis. *J Biol Chem*. 2008;283(48):33483–33497.
40. Sato H, et al. Group III secreted phospholipase A_2 transgenic mice spontaneously develop inflammation. *Biochem J*. 2009;421(1):17–27.
41. Masuda S, et al. Localization of various secretory phospholipase A_2 enzymes in male reproductive organs. *Biochim Biophys Acta*. 2004;1686(1–2):61–76.
42. Ensslin MA, Shur BD. Identification of mouse sperm SED1, a bimotif EGF repeat and discoidin-domain protein involved in sperm-egg binding. *Cell*. 2003;114(4):405–417.
43. Hellsten E, Evans JP, Bernard DJ, Jänne PA, Nussbaum RL. Disrupted sperm function and fertilin β processing in mice deficient in the inositol polyphosphate 5-phosphatase Inpp5b. *Dev Biol*. 2001;240(2):641–653.
44. Pearse RV 2nd, Drolet DW, Kalla KA, Hooshmand F, Bermingham JR Jr, Rosenfeld MG. Reduced fertility in mice deficient for the POU protein sperm-1. *Proc Natl Acad Sci U S A*. 1997;94(14):7555–7560.
45. Nayernia K, et al. Asthenozoospermia in mice with targeted deletion of the sperm mitochondrion-associated cysteine-rich protein (*Smcp*) gene. *Mol Cell Biol*. 2002;22(9):3046–3052.
46. Qi H, et al. All four CatSper ion channel proteins are required for male fertility and sperm cell hyperactivated motility. *Proc Natl Acad Sci U S A*. 2007;104(4):1219–1223.
47. Ikawa M, et al. Calmegin is required for fertilin α/β heterodimerization and sperm fertility. *Dev Biol*. 2001;240(1):254–261.
48. Stein KK, Go JC, Primakoff P, Myles DG. Defects in secretory pathway trafficking during sperm development in Adam2 knockout mice. *Biol Reprod*. 2005;73(5):1032–1038.
49. Sapiro R, Kostetskii I, Olds-Clarke P, Gerton GL, Radice GL, Strauss III JF. Male infertility, impaired sperm motility, and hydrocephalus in mice deficient in sperm-associated antigen 6. *Mol Cell Biol*. 2002;22(17):6298–6305.
50. Zhang Z, et al. A heterozygous mutation disrupting the SPAG16 gene results in biochemical instability of central apparatus components of the human sperm axoneme. *Biol Reprod*. 2007;77(5):864–871.
51. Tanaka H, et al. Mice deficient in the axonemal protein Tektin-t exhibit male infertility and immotile-cilium syndrome due to impaired inner arm dynein function. *Mol Cell Biol*. 2004;24(18):7958–7964.
52. Lorenzetti D, Bishop CE, Justice MJ. Deletion of the Parkin coregulated gene causes male sterility in the quaking(viable) mouse mutant. *Proc Natl Acad Sci U S A*. 2004;101(22):8402–8407.
53. Miki K, Willis WD, Brown PR, Goulding EH, Fulcher KD, Eddy EM. Targeted disruption of the Akap4 gene causes defects in sperm flagellum and motility. *Dev Biol*. 2002;248(2):331–342.
54. Ikeda K, Shimizu T, Taguchi R. Targeted analysis of ganglioside and sulfatide molecular species by LC/ESI-MS/MS with theoretically expanded multiple reaction monitoring. *J Lipid Res*. 2008;49(12):2678–2689.
55. Nakanishi H, Iida Y, Shimizu T, Taguchi R. Analysis of oxidized phosphatidylcholines as markers for oxidative stress, using multiple reaction monitoring with theoretically expanded data sets with reversed-phase liquid chromatography/tandem mass spectrometry. *J Chromatogr B Analyt Technol Biomed Life Sci*. 2009;877(13):1366–1374.
56. Sassone-Corsi P. Transcriptional checkpoints determining the fate of male germ cells. *Cell*. 1997; 88(2):163–166.
57. Escalier D. Knockout mouse models of sperm flagellum anomalies. *Hum Reprod Update*. 2006; 12(4):449–461.
58. Bailey RW, Aronow B, Harmony JA, Griswold MD. Heat shock-initiated apoptosis is accelerated and removal of damaged cells is delayed in the testis of clusterin/ApoJ knock-out mice. *Biol Reprod*. 2002; 66(4):1042–1053.
59. Butler A, Gordon RE, Gatt S, Schuchman EH. Sperm abnormalities in heterozygous acid sphingomyelinase knockout mice reveal a novel approach for the prevention of genetic diseases. *Am J Pathol*. 2007;170(6):2077–2088.
60. Murakami M, et al. Regulation of prostaglandin E_2 biosynthesis by inducible membrane-associated prostaglandin E_2 synthase that acts in concert with cyclooxygenase-2. *J Biol Chem*. 2000;275(42):32783–32792.
61. Ueno N, et al. Coupling between cyclooxygenase, terminal prostanoid synthase, and phospholipase A_2. *J Biol Chem*. 2001;276(37):34918–34927.
62. Fischer KA, et al. 15-Lipoxygenase is a component of the mammalian sperm cytoplasmic droplet. *Reproduction*. 2005;130(2):213–222.
63. Lazarus M, et al. Immunohistochemical localization of microsomal PGE sythase-1 and cyclooxygenases in male mouse reproductive organs. *Endocrinology*. 2002;143(6):2410–2419.
64. Law GL, McGuinness MP, Linder CC, Griswold MD. Expression of apolipoprotein E mRNA in the epithelium and interstitium of the testis and the epididymis. *J Androl*. 1997;18(1):32–42.
65. Hermo L, Wright J, Oko R, Morales CR. Role of epithelial cells of the male excurrent duct system of the rat in the endocytosis or secretion of sulfated glycoprotein-2 (clusterin). *Biol Reprod*. 1991; 44(6):1113–1131.
66. Morales CR, et al. ATP-binding cassette transporters ABCA1, ABCA7, and ABCG1 in mouse spermatozoa. *Biochem Biophys Res Commun*. 2008; 376(3):472–477.
67. Saez F, Frenette G, Sullivan R. Epididymosomes and prostasomes: their roles in posttesticular maturation of the sperm cells. *J Androl*. 2003;24(2):149–154.
68. Escoffier J, et al. Group X phospholipase A_2 is released during sperm acrosome reaction and controls fertility outcome in mice. *J Clin Invest*. 2010; 120(5):1415–1428.
69. Bligh EG, Dyer WJ. A rapid method of total lipid extraction and purification. *Can J Biochem Physiol*. 1959;37(8):911–917.
70. Houjou T, Yamatani K, Nakanishi H, Imagawa M, Shimizu T, Taguchi R. Rapid and selective identification of molecular species in phosphatidylcholine and sphingomyelin by conditional neutral loss scanning and MS3. *Rapid Commun Mass Spectrom*. 2004;18(24):3123–3130.
71. Taguchi R, et al. Focused lipidomics by tandem mass spectrometry. *J Chromatogr B Analyt Technol Biomed Life Sci*. 2005;823(1):26–36.
72. Fujino RS, Tanaka K, Morimatsu M, Tamura K, Kogo H, Hara T. Spermatogonial cell-mediated activation of an IkappaBzeta-independent nuclear factor-kappaB pathway in Sertoli cells induces transcription of the lipocalin-2 gene. *Mol Endocrinol*. 2006;20(4):904–915.